National Library of Canada
Bibliothèque nationale du Canada

Canadian Theses Service
Services des thèses canadiennes

Ottawa, Canada
K1A 0N4

CANADIAN THESES
THÈSES CANADIENNES

NOTICE

The quality of this microfiche is heavily dependent upon the quality of the original thesis submitted for microfilming. Every effort has been made to ensure the highest quality of reproduction possible.

If pages are missing, contact the university which granted the degree.

Some pages may have indistinct print especially if the original pages were typed with a poor typewriter ribbon or if the university sent us an inferior photocopy.

Previously copyrighted materials (journal articles, published tests, etc.) are not filmed.

Reproduction in full or in part of this film is governed by the Canadian Copyright Act, R.S.C. 1970, c. C-30.

AVIS

La qualité de cette microfiche dépend grandement de la qualité de la thèse soumise au microfilmage. Nous avons tout fait pour assurer une qualité supérieure de reproduction.

S'il manque des pages, veuillez communiquer avec l'université qui a conféré le grade.

La qualité d'impression de certaines pages peut laisser à désirer, surtout si les pages originales ont été dactylographiées à l'aide d'un ruban usé ou si l'université nous a fait parvenir une photocopie de qualité inférieure.

Les documents qui font déjà l'objet d'un droit d'auteur (articles de revue, examens publiés, etc.) ne sont pas microfilmés.

La reproduction, même partielle, de ce microfilm est soumise à la Loi canadienne sur le droit d'auteur, SRC 1970, c. C-30.

THIS DISSERTATION
HAS BEEN MICROFILMED
EXACTLY AS RECEIVED

LA THÈSE A ÉTÉ
MICROFILMÉE TELLE QUE
NOUS L'AVONS REÇUE

NL-339 (r.86/06)

Canada

THE UNIVERSITY OF ALBERTA

Bending Stresses Arising in Sucker Rod Ends

by

Richard Howe

(C)

A THESIS

SUBMITTED TO THE FACULTY OF GRADUATE STUDIES AND RESEARCH

IN PARTIAL FULFILMENT OF THE REQUIREMENTS FOR THE DEGREE

OF Master of Science

Department of Mechanical Engineering

Edmonton, Alberta

Spring 1987

Permission has been granted to the National Library of Canada to microfilm this thesis and to lend or sell copies of the film.

The author (copyright owner) has reserved other publication rights, and neither the thesis nor extensive extracts from it may be printed or otherwise reproduced without his/her written permission.

L'autorisation a été accordée à la Bibliothèque nationale du Canada de microfilmer cette thèse et de prêter ou de vendre des exemplaires du film.

L'auteur (titulaire du droit d'auteur) se réserve les autres droits de publication; ni la thèse ni de longs extraits de celle-ci ne doivent être imprimés ou autrement reproduits sans son autorisation écrite.

ISBN 0-315-37756-9

THE UNIVERSITY OF ALBERTA

RELEASE FORM

NAME OF AUTHOR Richard Howe

TITLE OF THESIS Bending Stresses Arising in Sucker Rod Ends

DEGREE FOR WHICH THESIS WAS PRESENTED Master of Science

YEAR THIS DEGREE GRANTED Spring 1987

Permission is hereby granted to THE UNIVERSITY OF ALBERTA LIBRARY to reproduce single copies of this thesis and to lend or sell such copies for private, scholarly or scientific research purposes only.

The author reserves other publication rights, and neither the thesis nor extensive extracts from it may be printed or otherwise reproduced without the author's written permission.

(SIGNED) .....

PERMANENT ADDRESS:

14707 101 ST.....

EDMONTON ALBERTA.....

.....

DATED APRIL 21 1987

THE UNIVERSITY OF ALBERTA

FACULTY OF GRADUATE STUDIES AND RESEARCH

The undersigned certify that they have read, and recommend to the Faculty of Graduate Studies and Research, for acceptance, a thesis entitled Bending Stresses Arising in Sucker Rod Ends submitted by Richard Howe in partial fulfilment of the requirements for the degree of Master of Science.

Arnold V. Bellows

Supervisor

Ramon Benteau

Gary Faulkner

Date April 15, 1987

Abstract

The purpose of this investigation was to examine bending stresses that occur near the upset bead as a result of small, pre-existing bends near the ends of sucker rods. These bending stresses arise when axial loads applied to a rod string cause an elastic "straightening" of the bent rod ends. The presence of large localized tensile bending stresses, in addition to the usual tensile stresses due to axial loading, may be a factor in the high percentage of sucker rod failures that occur near the rod end.

As a first step, a technique was developed to accurately measure existing bends in manufactured sucker rod ends. Subsequently, the measured rod ends were analysed with a numerical model to predict the bending stresses that would occur. The overall procedure was verified by comparing the experimentally measured bending strains for three pairs of connected rod ends with the strains predicted by the model.

The technique was then used to analyse a sample of ten rod ends. The rod ends came from a random sample of five, grade C quench and tempered, 3/4 inch (19 mm) diameter, six foot long (1760 mm) rods that were cut in half. Bending stresses ranging up to 68% of the axial stress were predicted for a 15 kips (66.9 KN) axial load.

In the overall analysis of the rod sample, a dimensionless bending stress, DB, was introduced to measure the magnitude of the bending stresses compared to the axial stresses.

Also, during the investigation, rod ends were tested and found to meet the American Petroleum Institute standard for rod straightness (API SPEC 11B, SEC 9.2.2, May 82). Application of the standard was concluded to be inadequate in limiting bending stresses to acceptable limits.

Acknowledgement

The author wishes to extend his appreciation to Dr D.G. Bellow for supervising this thesis, and to thank Dr D.R. Budney, Dr M.G. Faulkner and Dr F.H. Vitovec for advice received.

He would also like to thank the Mechanical Engineering Department of the University of Alberta for providing financial assistance for the study.

Finally, he is grateful to his wife and parents for their support during the writing of this thesis.

Table of Contents

Chapter		Page
1.	Introduction	1
	1.1 Nature of the Problem	1
	1.2 Thesis Outline	3
2.	Sucker Rod Operation	5
	2.1 Introduction	5
	2.2 Sucker Rod Strings	5
	2.3 Sucker Rod Pumping	7
	2.4 Sucker Rod Environment	10
3.	Review of Sucker Rod Research	12
	3.1 Introduction	12
	3.2 Prediction and Measurement of Nominal Stresses	12
	3.3 Reduction of Nominal Stresses	14
	3.4 Prediction and Measurement of Material Performance	15
	3.5 Improvement of Material Performance	16
	3.6 Elimination of the Problem Areas and "Weak Links"	18
	3.7 Experimental Research of the Thesis	19
4.	Method of Analysing Non-straight Rod Ends	21
	4.1 Introduction	21
	4.2 Numerical Model to Analyse Non-straight Rod Ends	24
	4.2.1 Description of Theoretical Model	24
	4.2.2 Numerical Solution of Theoretical Model	26
	4.3 Measurement of the Initial Bend	30
	4.3.1 Introduction	30
	4.3.2 Measuring Procedure	32

5. Experimental Verification of Model 37

5.1 Experimental Procedure 37

5.2 Experimental Results 38

6. Analysis and Discussion of Results 46

6.1 Introduction 46

6.2 Analysis of Selected Rods 47

6.2.1 Stress Distribution Along Rod 47

6.2.2 Factors Affecting the Bending Stress 47

6.3 Analysis of the Overall Sample 54

6.3.1 Distribution of Bending Stresses in the Sample 54

6.3.2 Limitations of Current Standards 56

6.3.3 Evaluating Rod End Straightness 58

7. Conclusions 62

Bibliography 63

Appendix 1: API Sucker Rod Grades 69

Appendix 2: Sucker Rod Failure Mechanisms 70

Appendix 3: Least Squares Analysis 82

Appendix 4: Difference Equations, Coordinate Transforms, and Program Description 84

List of Tables

Table		Page
1.	Experimental vs. Predicted Strains	41

List of Figures

Figure		Page
1.	Forged and Machined End of Sucker Rod	6
2.	Sucker Rod Coupling	6
3.	Rod Pumped Well	8
4.	Load Cycle on Rod String	9
5.	Rod End	22
6.	Non-Straight Rod End	22
7.	Bar Deflected Under Axial Load	22
8.	Bar with Uniform Cross Section with a Sharp Bend	25
9.	Free Body Diagram of a Section of Bent Rod Axially Loaded	25
10.	Representation of Connected Rods in the Numerical Model	28
11.	Comparison of Numerical Solution to Analytical Solution for a Bar with a Sharp Bend	29
12.	Angle and Magnitude of Deviation at a Cross Section of Rod	31
13.	Mapping of Coordinates of Measured Rods to a Global Coordinate System for Solution	31
14.	Rod and Coupling Mounted in Lathe for Measuring Deviation	33
15.	Measurement Error Created by a Non-Circular Cross Section	34
16.	Finding the Vertical Deviation, R_i, for a Rotation Angle, α_i	34
17.	Schematic of Data Acquisition System	36
18.	Rods Mounted in Tensile Testing Machine	39
19.	Ball and Socket Connection For Mounting Rods	40
20.	Comparison of Numerical Solution to Experimental Measurements - 4a 2a Combination	42

21. Comparison of Numerical Solution to Experimental Measurements - 4a 3a Combination.....43

22. Comparison of Numerical Solution to Experimental Measurements - 4a 5a Combination.....44

23. Stress Distribution Along Length of Connected Rods - 4a 2a Combination.....48

24. Stress Distribution Along Length of Connected Rods - 4a 3a Combination.....49

25. Stress Distribution Along Length of Connected Rods - 4a 5a Combination.....50

26. Range of DB_{34} for Rod 5a 52

27. Variation of DB_{34} due to Variation of Twist Angle of Connection.....53

28. DB_{34} Frequency Plot for Rod Connections Made from Rods in Sample.....55

29. Comparison of TIR Measured by API Methods to DB_{34} 57

30. Comparison of TIR Measured at Four Inches to DB_{34} 59

31. Design Chart for Upper-Limit Stresses in Rod Sample.....60

I. Calculation of Time to Failure for Stage II Crack Propagation.....72

II. Relationship of α_i and R_i to R and θ 82

III. Node i with Adjacent Beam Elements.....84

Nomenclature

A	Area of a cross section.
DB	Dimensionless bending stress defined as $\sigma_{bending}/\sigma_{axial}$.
DB_{34}	Dimensionless bending stress for an axial stress of 34 ksi(235 MPa).
E	Modulus of elasticity.
I, I_i	Moment of inertia at a cross section and at a cross section in element i.
M	Bending moment.
P	Axial load.
R	Magnitude of deviation of a centroid of a cross section from the centre line through the pin.
R_a	Assumed magnitude of deviation using a single measurement.
R_i	Vertical deviation of a centroid of a cross section from the centre line through the pin for a given angle of rotation, α_i.
TIR	Total indicator runout, API measure of rod end straightness.
X_1, Y_1, Z_1	Coordinate axes for the first rod in the numerical model.
X_2, Y_2, Z_2	Coordinate axes for the second rod in the numerical model.
X_G, Y_G, Z_G	Global coordinate axes for the numerical model of two connected rods.
a	Distance from end of bar to sharp bend in bar.
d	Distance measured from datum line to rod surface.
d_{180}	Distance measured from datum line to rod surface after rotating rod 180 degrees.

dd	Distance of datum line from the centre line through the pin.
h_i	Length of element i.
l	Length of bar.
n	Number of elements in numerical model.
r	Radius of a cross section.
x, y	Deviation in the x and y directions of the cross section centroid from the global z axis for the deflected position of the rod.
x_i, y_i	Deviation in the x and y directions of the cross section centroid of node i from the global z axis for the deflected position of the rod.
x_o, y_o	Deviation in the x and y directions of the cross section centroid from the global z axis for the undeflected position of the rod.
x_{o_i}, y_{o_i}	Deviation in the x and y directions of the cross section centroid of node i from the global z axis for the undeflected position of the rod.
(x_o-x), (y_o-y)	Deflection of a cross section centroid from the undeflected position (x_o,y_o) in the x and y directions.
z	Distance along the length of the bar from the origin.
z_0, z_n	Origin and end of bar model.
α_i	Angle of lathe rotation for a given measurement of vertical deviation, R_i.
ϵ_{axial}	Tensile strain due to axial load, P.
$\epsilon_{bending}$	Tensile strain due to bending moment, M.
$\epsilon_{bending}/\epsilon_{axial}$	Strain ratio.
γ	Angle (in radians) of a sharp bend in a bar measured from the centre line through the ends.

θ	Angle, measured from the x axis, of the deviation of the cross section centroid from the global z axis.
σ_{axial}	Tensile stress due to axial loading.
$\sigma_{bending}$	Tensile stress due to bending moment.
σ_{total}	Total tensile stress due to both the axial load and the bending moment.

1. Introduction

1.1 Nature of the Problem

After an oil reservoir is discovered, the main objective is to produce as much of the oil as possible in the most economical manner. Because of a lack of natural energy, many producing wells use some method of artificial lift for bringing the oil to the surface. Due to its efficiency, serviceability, and flexibility, the sucker rod pumping system has traditionally been the preferred method of artificial lift; 80% of all oil wells either begin production with or eventually use a sucker rod pumping system (Zaba, 1962). In this system, a sucker rod string, often over a mile(1.6 km) in length, is used to pull the oil to the surface. Unfortunately the sucker rod strings occcasionally break. The result is lost revenue due to downtime and increased expenses due to repair costs. In many instances, the frequency of breakage can become a significant factor in the overall economics of a well.

On first examination, the problem appears simple; a long round bar is loaded with a column of oil resulting in an axial stress. Since the maximum nominal stress [1] can usually be limited to below 34 ksi(235 MPa) by appropriate selection of rod sizes, the obvious solution is to use a steel that will not break at this stress. While most steels can withstand several times this stress, none of them are

---

[1] The nominal stress refers to the average tensile stress in the main body of the sucker rod.

immune to failure when used in a sucker rod string. Thus the problem is more complicated than is at first apparent.

There are three factors that complicate the problem and contribute to sucker rod failures. First, the loading on the rod string is not constant but undergoes a cyclic variation due to the reciprocating motion of the rod string. The resulting cyclic stresses can lead to fatigue failure. Second, the rod string is exposed to well fluids that can sometimes be sour[2] and/or corrosive. These damaging environments interact synergistically with the fatigue process resulting in several possible failure mechanisms depending on the kinds of interaction. Third, pre-existing imperfections in the manufactured rods can lead to localized stresses in the rods which are larger than the assumed nominal stresses. When high localized stresses occur, they can be an important factor in initiating fatigue failures.

The question of sucker rod failures has been actively researched since the 1930's resulting in several major improvements in rod string performance. In particular, improvements in the rod connections have dramatically increased the overall service life of rod strings. Yet rod string failures remain common especially as deeper and more severe well environments are encountered. Research aimed at further improving rod string performance can take one of three directions:

1. The loading conditions under which rod strings operate

---

[2]Sour is a term used to describe a well containing hydrogen sulphide gas.

can be improved. Research in this area is limited mainly to improving the operating procedures of sucker rod wells.

2. The general performance of the rod material can be improved. Much of the research in this area must further delineate the actual failure mechanisms occurring in rod strings in the different types of well environments.
3. The remaining "weak links" can be eliminated. Research in this area must first identify and then explain any "weak links" that still exist.

The experiments discussed in this thesis are an aspect of this third line of research.

1.2 Thesis Outline

The first part of the thesis consists of a general review of sucker rods and of sucker rod research. In Chapter II, a general description of sucker rod strings and sucker rod pumping is followed by a review of the types of environments to which sucker rods are exposed. The purpose is to illustrate the constraints and conditions under which rod strings operate. Chapter III opens with a literature review on methods for predicting, measuring, and increasing the service life of rod strings. This chapter finishes by putting the experimental work of the thesis in context with previous research on sucker rods.

The second part of the thesis deals with some experiments conducted on sucker rods. Bending stresses near

the upset end of the sucker rod had been previously proposed as a cause for a high frequency of failures in the same area (Bellow,1981). This thesis examines bending stresses arising from pre-existing bends in typical manufactured sucker rods. Chapter IV discusses the development of a numerical model to analyse bending stresses in non-straight sucker rods. An experimental technique is also introduced for measuring small bends in actual rods. In Chapter V, experiments measuring the bending strains in actual rods are described which verify the numerical model and measurement techniques in Chapter IV. Chapter VI presents an analysis of selected rods to show the complex nature of the bending stresses that arise. The chapter also presents an overall analysis of the measured sample of rods to give an indication of the extent to which bending stresses may occur in actual rod strings. The overall analysis is also used to evaluate current American Petroleum Institute (API) standards on bent rods. In the last chapter, Chapter VII, the conclusions of the experimental research are presented.

2. Sucker Rod Operation

2.1 Introduction

Before examining sucker rod failures, the conditions and constraints of sucker rod operation must be understood. This chapter begins with a brief description of a sucker rod string followed by an examination of sucker rod pumping. The last section examines the effects that oil well fluid properties have on rod string service life.

2.2 Sucker Rod Strings

Though continuous steel rod strings and rods made of fibreglass have been introduced, the 25 ft(7.6 m) steel sucker rod continues to be the most common component used in making up rod strings. A typical string will contain several hundred such sucker rods connected by couplings. Economy, flexible utilization, and proven performance are the major reasons for the continued popularity.

Manufactured from bar rounds, with diameters from 1/2 in.(12.7 mm) up to 1 1/8 in.(28.6 mm), the rod is forged and machined to create a roll-threaded pin, shoulder, wrench square, and upset bead at each end (Fig. 1). The coupling, which connects the pins of adjacent rods, consists of a short round steel cylinder which is bored through and machined with an inside rolled thread (Fig. 2).

Standards for rod manufacturing are set by the American Petroleum Institute (API, 1982) and are basically intended

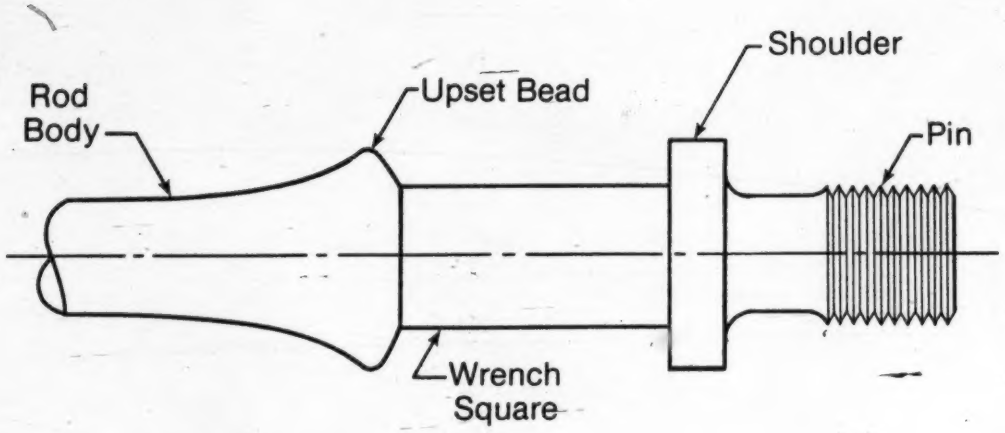

Fig. 1. Forged & Machined End of Sucker Rod

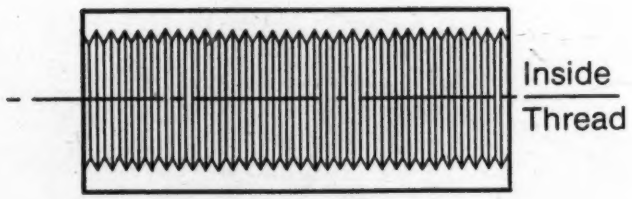

Fig. 2. Sucker Rod Coupling

to cover dimensional geometry. Requirements for the type of steels and heat treatments to be used are very broad, mainly requiring the class of steel and the ultimate tensile strength to fall within a given range for each grade of rod (Appendix 1). Manufacturers of the prevalent API grade C rods typically use an AISI 1036 normalized steel with a minimum ultimate tensile strength of 90 ksi(620 MPa).

2.3 Sucker Rod Pumping

Simply put, an oil well is a pipeline extending from the oil reservoir up to the surface. Commonly referred to as a tubing string, this pipeline typically consists of several hundred 25 ft(8.3 m) sections of 2-3/8 in.(60 mm) steel tubing suspended in a bore hole lined with 7 in.(178 mm) steel casing pipe. At the level where the formation is to be produced, the casing is perforated to allow well fluids to enter the well bore from the surrounding rock.

In most wells, the fluids entering the well bore are lifted to the surface by a rod string actuating a ball-valve pump at the bottom of the tubing string (Fig. 3). At the surface, a pump jack pulls the rod string up and down inside the tubing. When the upstroke begins, the traveling valve closes thereby transferring the fluid load to the rod string (Fig. 4a). During the upstroke, the fluid column is pulled up by the rod string (Fig. 4b). When the downstroke begins, the traveling valve opens and the standing valve closes thereby transferring the fluid load back to the tubing (Fig.

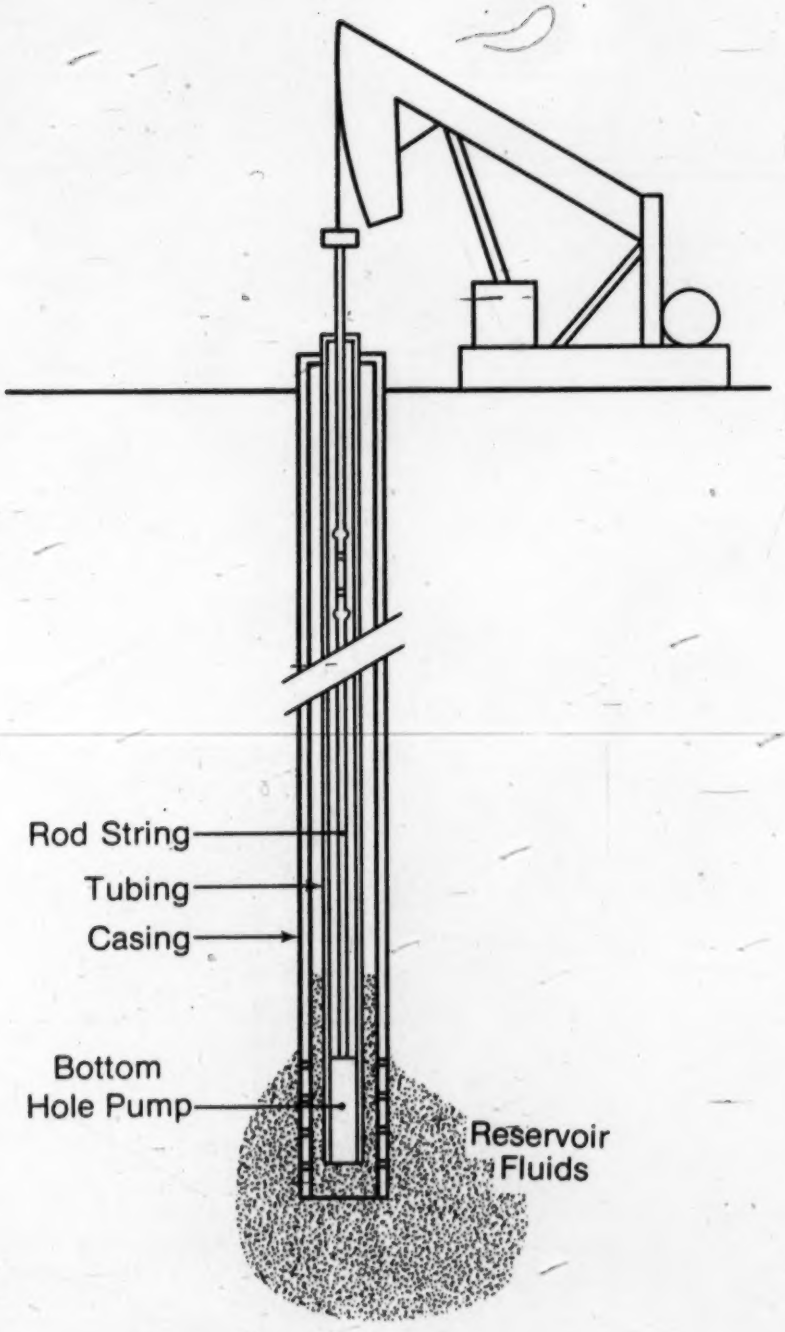

Fig. 3. Rod Pumped Well

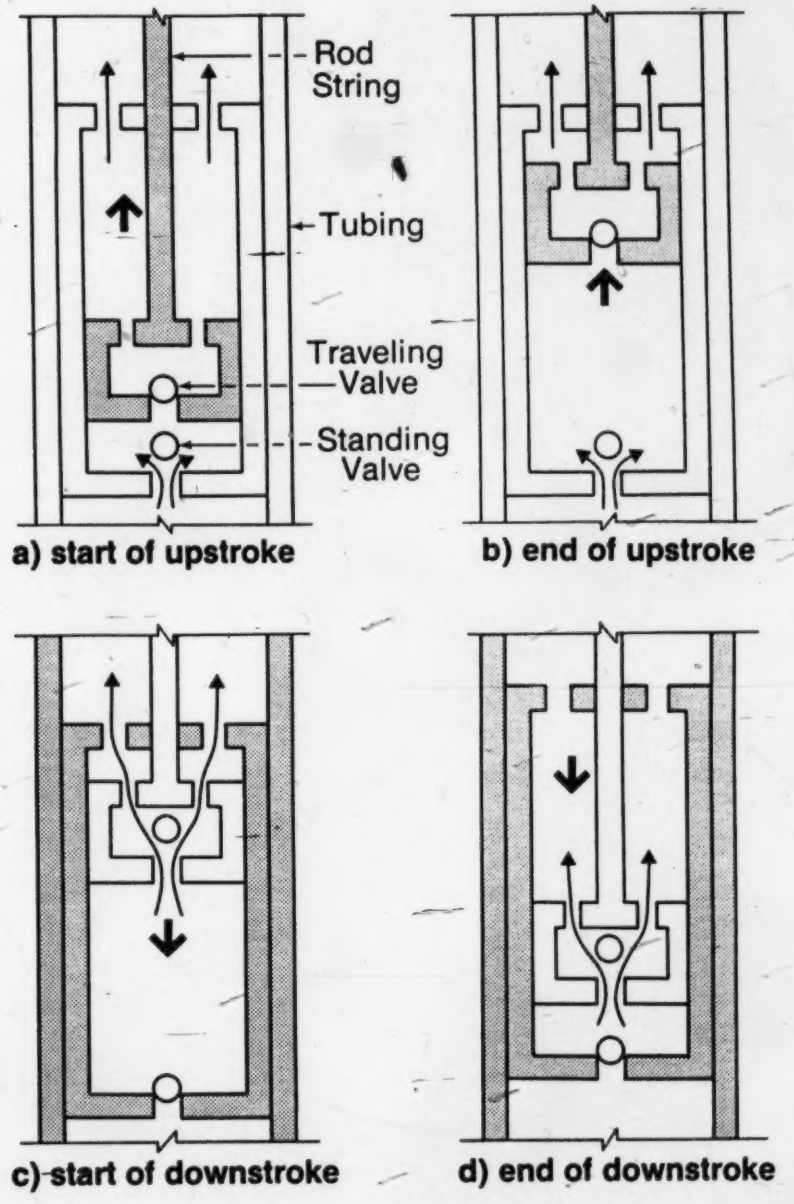

*loaded structures are shaded

Fig. 4. Load Cycle on Rod String

4c). During the downstroke, the rod string falls through the fluid column to restart the cycle (Fig. 4d). Both the tubing and the rod string experience a cyclic loading but the range of stresses is much higher in the rod string. This is due to the acceleration and deceleration of the moving rod string, to the smaller cross sectional area of the rods, and to the fact that the tubing is usually anchored at the well bottom. Operating at ten strokes per minute, a typical pump jack will subject the rod string to over ten million load cycles over a two year period (wells are often in production for twenty years or more).

2.4 Sucker Rod Environment

The properties of the oil well fluids can have a large influence on the service life of a rod string. When the water component (brine) of the pumped fluids is corrosive, a synergistic failure mechanism known as corrosion fatigue can greatly reduce the service life. Furthermore, the effects are more severe than can be explained by simply adding the damage from corrosion to the fatigue process. The presence of H_2S also plays an important role in reducing rod string service life, though the exact details of the interaction are even less known than in corrosion fatigue. In both cases of damaging environments, the endurance limit [3] is removed.

---

[3]The endurance limit is the maximum cyclic stress that can be applied for an infinite number of cycles. In normal fatigue failure of unnotched steels, cyclic stresses that do not cause failure in ten million cycles will never cause failure.

This means that even very low cyclic stresses will cause failure if enough time has elapsed. Though the details of sucker rod failure mechanisms are complex (Appendix 2), one important factor should be noted; stress plays a central role in both damaging and non-damaging environments.

3. Review of Sucker Rod Research

3.1 Introduction

Research directed at improving the service life of rod strings has covered a diverse range of subjects. This review examines the major areas of the published research in an attempt to relate the separate efforts and to put the thesis experimental work in context. For the purposes of this review, sucker rod research has been classified in the following five categories:

1. Prediction and measurement of nominal stresses
2. Reduction of nominal stresses
3. Prediction and measurement of material performance
4. Improvement of material performance
5. Elimination of the problem areas and 'weak links'

3.2 Prediction and Measurement of Nominal Stresses

Predicting the stresses in a mile-long (1.6 km) rod string is a mathematically difficult problem to solve. Originally, rod strings were analysed as a simple single degree of freedom spring-mass model (Coberly,1938). Measurements from operating oil wells were then combined with the simplified model to obtain an empirical expression for predicting the rod stresses (Mills,1943,Thompson,1959). Later on, Gibbs (1963) modeled the rod string as a continuous elastic structure using a one-dimensional wave equation allowing for the effects of viscous damping by the

fluid column. Electric analog computers were used to develop a series of solutions to a model similar to the one proposed by Gibbs (Midwest Research Inst.,1968). The design approach developed from the solutions was included in the recommended practices of API (API,1970). One study (Griffin,1968) found the newer methods to be only a slight improvement over the earlier Mills formula (Mills,1943) for predicting stresses in actual wells. A recent digital computer model proposed by Doty (1983) takes into account additional factors including the dynamics of the fluid column and the tubing string, and has shown good correlation with field measurements in a preliminary study (Doty).

Methods for measuring the loads and displacements of the polished rod * with a dynamometer and the displacements of the pump with a bottom-hole dynagraph were first developed by Gilbert (1936). The measurement of rod string dynamics was greatly simplified by the introduction of the "Delta II" dynamometer test (Gibbs,1966). Using a computer analysis of the polished rod loads and displacements, stresses anywhere within the rod string can be determined. The technique eliminates the need for a pump dynagraph which requires that the rod string be pulled.

---

*The polished rod is the first rod in the rod string and connects the rest of the rod string to the pump jack.

3.3 Reduction of Nominal Stresses

Reduction of rod string stresses has proven to be an effective technique in reducing overall rod failures in both corrosive and non-corrosive environments. Field studies by Dale & Johnson (1940) and Atkinson (1960) showed significant reductions in rod failures when stress levels were reduced in corrosive wells. A later study by Holliman & others (1966) showed similar results in non-corrosive wells.

The primary method of reducing the mean stress is to use a tapered string, in which the diameter of the deeper rods is smaller than the diameter of rods closer to the surface. This reduces the mean stress in the top rods which are carrying the weight of the rod string in addition to the fluid load.

Shock absorbers, first proposed by Eaton (1936), and hi-slip electric motors are both intended to smooth out the rod string load cycle thereby reducing the amplitude of the stress fluctuations. Field studies of shock absorbers (Holliman & others,1966) and hi-slip motors (Baron,1980) have reported success in reducing the polished rod stress ranges. The amplitude of stress fluctuations can also be reduced by using a longer pump stroke to reduce acceleration loads. New pump designs have been introduced to give strokes of up to 34 ft(10.4 m) (Ewing,1971).

Probably the most effective approach to reducing the nominal stresses involves proper design and operation of the beam-pumping system. In a West Kansas study (Atkinson,1960),

significant reductions in overall stress levels were achieved by using actual load measurements to redesign the pumping systems and to modify the operating parameters. A field study by Holliman (1966) found that paraffin accumulations and tight clearance pumps had resulted in an increased range of stresses. In some instances, compressive stresses were occurring causing the rod string to buckle on the downstroke. Amezcua (1980) found improvements in rod string service when fluid pound conditions were eliminated. Fluid pound is a condition that occurs when a well is pumped at a rate fast enough to prevent complete filling of the pump barrel. On the downstroke, a shock loading occurs when the pump hits the fluid surface of the partly filled pump barrel.

3.4 Prediction and Measurement of Material Performance

Methods to improve material performance in a given environment under a given stress history usually have substantial associated costs. Therefore, it is imperative that the material performance be accurately predicted and measured in order to determine the net gains. Much of the data on sucker rod performance in non-damaging environments has been compiled in the API modified Goodman charts (API, 1969) for use in design.

On the other hand, very little has been published on the actual performance of different rod materials in specific corrosive and sour environments. One set of mixed

rod string tests [1] by Atkinson (1960), showed that the type of steel used in a sucker rod had little effect on the service life of a rod in a corrosive environment. This study only covered a small subset of the conditions possible in oil wells. There have been many laboratory studies of rod string performance in sour and/or corrosive environments but the results correlate poorly with the actual performance in the field. The poor correlation between laboratory and field occurs because the long time durations and exact conditions of the actual applications are hard to duplicate in laboratory experiments (Zaba,1962).

3.5 Improvement of Material Performance

Organic inhibitors were the first (Pearson,1948) and are still the most common method used to extend rod life, yet some producers still question whether the benefits justify the additional costs. The basic concept of inhibitors is to place a protective barrier between the rod surface and the well environment (Nestle,1973), but it has been found generally that the tubing string is protected better than the rod string (Mehdizadeh & McGlasson,1967, McReynolds & Vennet,1975). The use of inhibitors that prevent hydrogen penetration of steel (Martin,1980) and the use of continuous monitoring to maintain inhibitor protection (Shehorn,1980) both show promise in specifically

---

[1] A mixed rod string test is carried out by installing rod strings made up of a random mix of the different types of sucker rods being tested. The performance of the different types of sucker rods are then monitored.

protecting sucker rods.

Closely related to the use of inhibitors is the use of epoxy coatings bonded to the rod surface. Originally introduced to replace metal and plastic scrapers in preventing paraffin buildups, studies showed that the coatings also resulted in extended rod life (Crevolin,1980). Since the coating is expensive, more research is needed to determine the extent of the protection in different environments.

The substitution of different materials for the regular rod steels has been attempted from the time steel rods first replaced wooden rods. Fibreglass rods (Detterick & Saul,1980) have recently been introduced to increase production and to eliminate the effects of damaging environments. Problems in handling large loads and high initial costs limit their application at present.

The final method of improving material performance involves improving the surface qualities of the sucker rod steel. Induction hardened (Glickman,1962) and shot peened surfaces (Mehdizadeh,1974) have both shown potential for resisting fatigue in damaging and non-damaging environments. Induction hardened rods, though, have initially shown quality control problems (Atkey & MacDonald,1980).

3.6 Elimination of the Problem Areas and "Weak Links"

Early problems with rod strings focused on connection failures at the pin threads and in the couplings. The introduction of the undercut pin (Vollmer,1952) and rolled threads (Crosby,1970) greatly improved the fatigue limit of the connection. Over the same period, a gradual evolution of connection make-up practices resulted in reduced fatigue loading of the connection. A recent study (Steward,1973) found that connection failures accounted for only 20% of the total rod failures. Currently, some producers feel that connection failures can be eliminated when proper installation procedures (API,1973) are followed.

Raised stresses from sucker rods bent in the field (Bellow & Kumar,1978, Chastain,1977) and microcracks resulting from hammering on the sucker rods (Chastain) have been blamed in many failures. The striking of weld arcs during the installation of metal scrapers is one of the few manufacturing defects cited for causing failures (Atkey & MacDonald,1980). Experience in pipelines had previously shown that the striking of a weld arc could result in the formation of a microcrack. Breaks resulting from rolling defects and forging laps are rare occurrences (Atkey & MacDonald).

3.7 Experimental Research of the Thesis

One of the remaining "weak links" to be explained occurs at the junction of the upset bead with the rod body. Maradudin (1965) reported that 20% to 30% of all rod string failures occurred near this junction. Dvoracek (1973) later reported that 75% of all the failures within the rod body happened near the upset end (Union Oil wells). In one test study of 60 rods, Bellow (1981) found that 43 of the failures occurred in this same region.

The authors of a Russian paper (Makarov & others,1981) found that metallurgical changes took place and that residual stresses were introduced as a result of heating and, subsequently, forging the rod end. Using x-ray diffraction techniques, the study reported the occurrence of surface residual tensile stresses that were as high as 70% of the yield strength. The study also reported increased grain size in the region of the rod subjected to heating during forging. The study was based on Russian manufactured sucker rods; no comparable study based on North American rods has been published.

Bellow (1981) had previously proposed that bending stresses due to misalignments between the test rods and the test apparatus were the cause for the high proportion of failures near the upset end in his experiments. The misalignments were due to test rods not being straight. A recently published Chinese study (Li,1984) reported that during axial loading, bending stresses were found near the

upset end of sucker rods with bent rod ends. The authors of the study were not successful in relating the degree of bend existing in the rods to the resulting bending stress, though the authors did establish upper and lower limits for the stresses.

The purpose of this study was to examine the bending stresses which occur near the upset bead as a result of non-straight rod ends. A method was first developed to measure the actual bends that occur in manufactured rods. Using the measured bends, a numerical model was then used to predict the bending stresses that would occur under axial loading conditions similar to loading conditions in the field. For an axial load of 15 kips(66.9 KN), bending stresses up to 68% of the nominal axial stress were predicted (Chapter VI). The finding of high bending stresses is significant because of the role that stress plays in sucker rod fatigue failures in both damaging and non-damaging environments.

4. Method of Analysing Non-straight Rod Ends

4.1 Introduction

For the purposes of this study, a rod end is defined as a section of sucker rod extending from the shoulder to a point approximately thirty-four inches (860 mm) back onto the rod body (Fig. 5). The rod end is defined as non-straight if it deviates from a hypothetical centre line extending through the pin (Fig. 6). In general, the extent of the deviation in the rod end is small; usually, the rod end will appear straight upon visual inspection.

To analyse the stresses occurring in a non-straight rod end, elementary beam theory is used together with the equation for uniform stresses in a bar subjected to an axial load where

$$\sigma_{bending} = Mr/I \text{ and } \sigma_{axial} = P/A \text{ with}$$

M = bending moment,
r = cross section radius,
I = moment of inertia,
P = axial load,

and

A = cross sectional area.

The bending moment at any cross section is simply

$$M = Py$$

where y is the deflected distance of the cross section centroid from a centre line passing through the applied load (Fig. 7).

The details of determining the final deflected position will be left for the next section, but a simple calculation

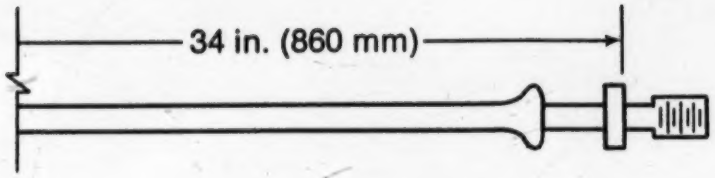

Fig. 5. Rod End

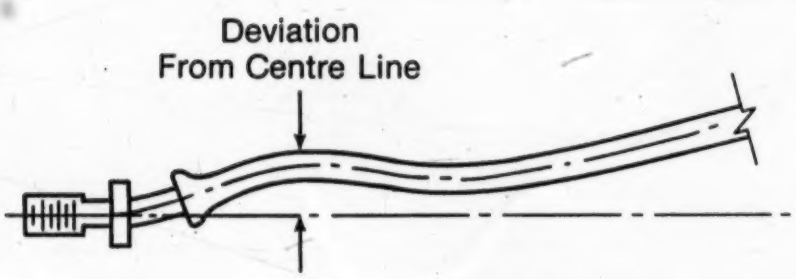

Fig. 6. Non-Straight Rod End

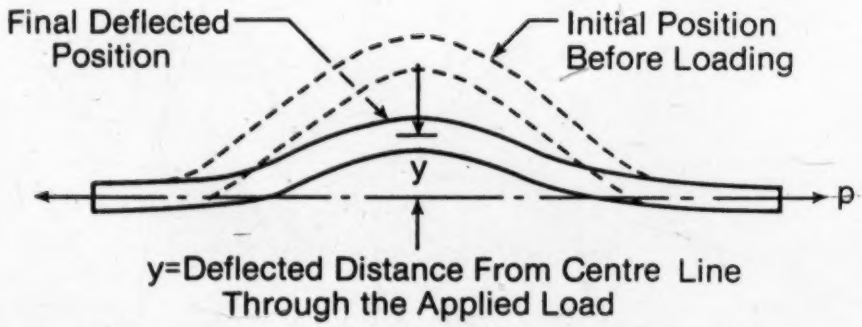

Fig. 7. Bar Deflected Under Axial Load

can be made to determine the size of deviation (after deflection) that is significant. Using a rod diameter of 0.75 in.(19 mm) and a load of 15000 lb(66.9 KN), conditions typical in an operating rod string, the parameters are

$$r = 0.375 \text{ in.} \quad A = 0.442 \text{ in.}^2 \quad I = 0.0155 \text{ in.}^4$$

which yields a bending stress equal to 363y ksi and an axial stress equal to 33.9 ksi(234 MPa). If the final deflected position at a cross section is one-sixteenth of an inch(1.6 mm) from the centre line, the bending stress will be 22.7 ksi(156 MPa) which is 67% of the axial stress. Clearly, small deviations of the rod from the centre line have the potential to create large bending stresses if the rod does not straighten under the axial load‘.

When examining stresses occurring in non-straight rod ends, the dimensionless bending stress, DB, is of use for determining the relative importance of the bending stresses as compared to the axial stresses. In this study, DB is defined as the stress due to bending divided by the stress due to the axial load:

$$DB = \sigma_{bending}/\sigma_{axial}.$$

For a non-straight rod end where the bending moment arises from the axial load the DB can be simplified to

---

‘ The concept of straightening under the load refers to a temporary elastic deflection and should not be confused with permanent plastic deformation. Any attempt to straighten a rod end that uses permanent plastic deformations will result in high residual stresses (Bellow, 1979).

$$DB = (Pyr/I)/(P/A) = 4y/r \ .$$

4.2 Numerical Model to Analyse Non-straight Rod Ends

4.2.1 Description of Theoretical Model

In the preceding section the basic concepts for analysing non-straight rod ends were introduced. This section introduces the differential equation used to describe the final deflected position of a non-straight bar subjected to an axial load. The equation was used successfully by Bellow (1979) to predict stresses in bars of uniform cross section with a sharp bend (Fig. 8).

The differential equation is derived from the free body diagram in Fig. 9 where

$$M = Py$$

and from the elementary theory of deflection of a beam where

$$M = -EI\frac{d^2(y_o-y)}{dz^2} \ .$$

In the above equation, (y_o-y) represents the deflection of the bar from the unloaded position. Equating the moments and rearranging the terms results in the following differential equation:

$$\frac{d^2y}{dz^2} - \frac{P}{EI}\,y = \frac{d^2y_o}{dz^2}.$$

Similarly in the x direction, the equation becomes

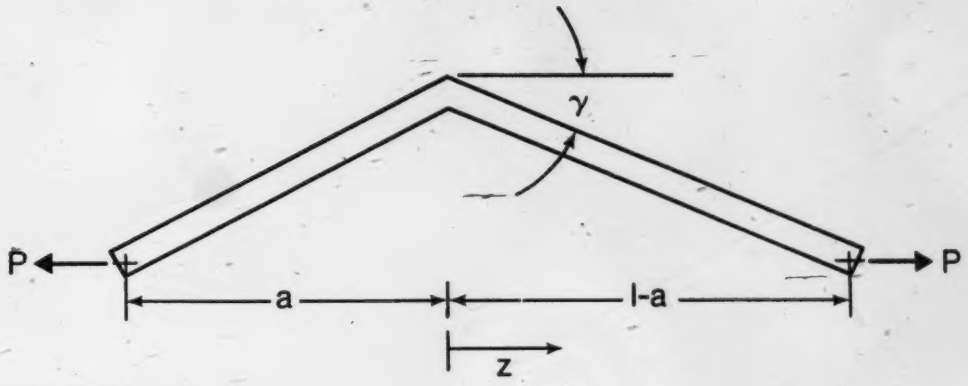

Fig. 8. Bar With Uniform Cross Section With a Sharp Bend

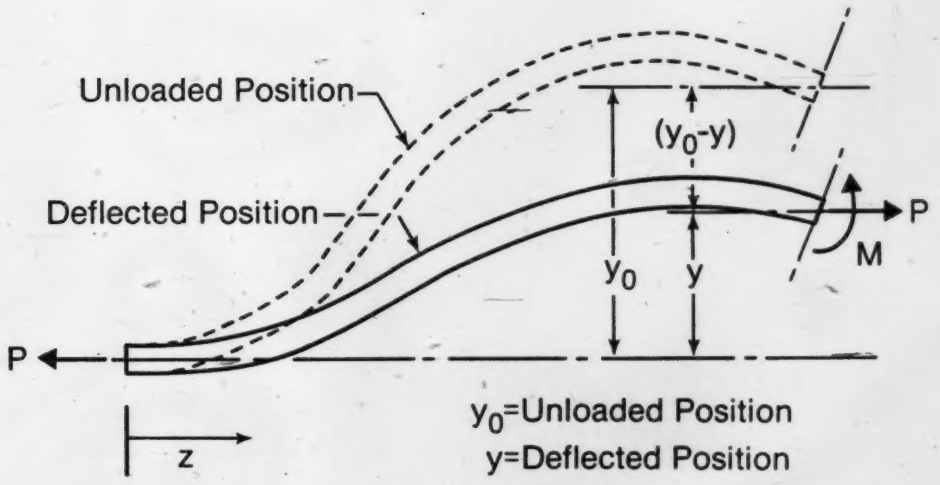

Fig. 9. Free Body Diagram of a Section of Bent Rod Axially Loaded

$$\frac{d^2x}{dz^2} - \frac{P}{EI} x = \frac{d^2x_o}{dz^2}.$$

For a non-straight rod the DB at any cross section can be determined from the final deflected position with the following equation,

$$DB = \frac{4}{r} (x^2+y^2)^{\frac{1}{2}}.$$

This equation is similar to the previous equation derived for bending about the x-axis only.

4.2.2 Numerical Solution of Theoretical Model

To analyse stresses in a non-straight rod, the differential equation must be solved for the case of a changing cross section and an arbitrary initial bend in three dimensions. Since analytical solutions are not possible for this general case, a numerical approach must be used to solve for the deflections. Towards this end, the equations are recast into the following finite difference form for the y-direction

$$\frac{y_{i+1}}{h_{i+1}} + \frac{y_{i-1}}{h_i} - \left[\frac{h_i+h_{i+1}}{h_i h_{i+1}} + \frac{h_i I_{i+1}+h_{i+1} I_i}{2EI_i I_{i+1}} P\right] y_i = \frac{y_{o_{i+1}}}{h_{i+1}} + \frac{y_{o_{i-1}}}{h_i} - \frac{h_i+h_{i+1}}{h_i h_{i+1}} y_{o_i}$$

and in an identical form for the x-direction to permit a numerical solution (Appendix 4). These formulations are specific to a case such as a rod string where no moments are imposed at the ends of the bar; the only force applied is the axial load. The boundary conditions become

$$y = 0 \text{ at } z = z_0 \quad \text{and} \quad y = 0 \text{ at } z = z_n.$$

For an n-element model, the solution reduces to the solution of two independent sets of (n-1) linear equations each with (n-1) unknowns.

The specific computer model developed to analyse the connection of two rods utilized seventy elements of unequal size; small elements were used in areas of rapidly changing cross section and in the expected areas of rapidly changing bending moments whereas larger elements were used elsewhere to reduce computation time. The model idealizes the connection of two rods as a sixty-four inch(1625 mm) long, non-uniform bar axially loaded at each end (Fig. 10). The cross sectional changes through the upset forged region and the coupling are included within the model. A description and listing of the subroutines used to set up and solve the model are included in Appendix 4.

The numerical model was initially tested by comparing the numerical solution for a sharply bent bar with uniform cross section (Fig.8) to the analytical solution for a nearly identical problem with one exception; the numerical model used a finite length of sixty-four inches(1526 mm) while the analytical solution is for a bar of infinite length. The analytical solution, verifiable by back substitution, is

$$(EI/P)^{1/2}\gamma EXP\{-(P/EI)^{1/2}z\} = y$$

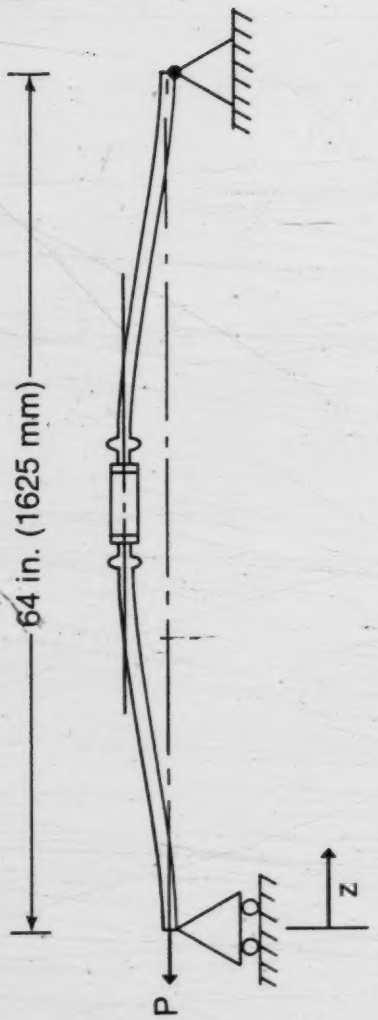

Fig. 10. Representation of Connected Rods in the Numerical Model

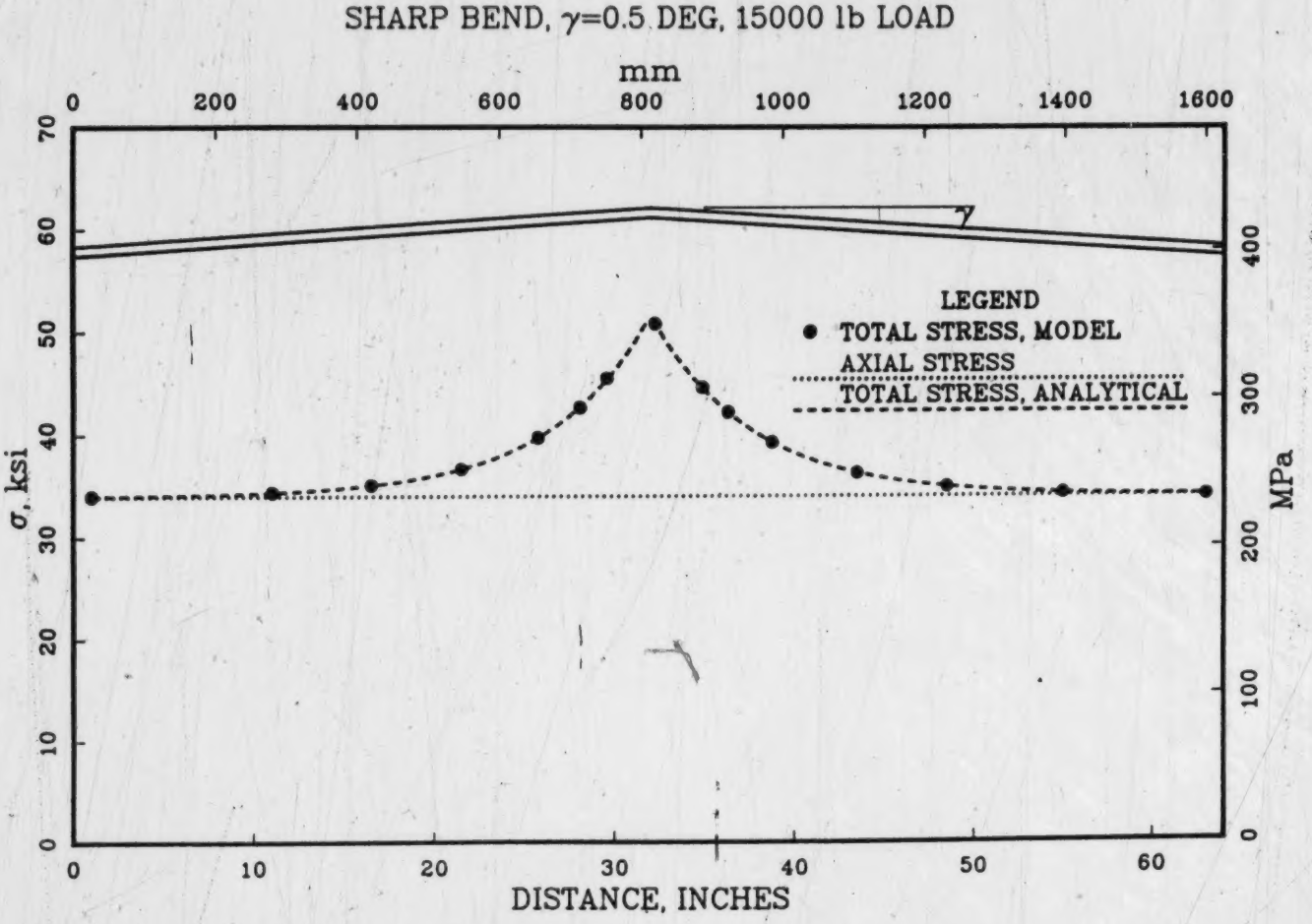

Fig. 11. Comparison of Numerical Solution to Analytical Solution for a Bar with a Sharp Bend

which also satisfies the boundary conditions

$$\frac{d^2y_o}{dz^2} = 0, \quad \frac{dy}{dz} = -\gamma \text{ at } z = 0, \text{ and } y = 0 \text{ at } z = \infty.$$

In Fig. 11, the agreement between the two solutions is shown to be extremely close; apparently, the use of a finite section of bar to model an infinite rod string is valid if the bend (after deflection) is confined to the central section of the finite length model.

4.3 Measurement of the Initial Bend

4.3.1 Introduction

The next step in analysing the bending stresses was to develop a procedure for measuring the pre-existing bends occurring in actual rod ends. The strategy was to determine, at different locations along the length of the rod end, both the magnitude of the deviation, R, from a centre line through the pin and the angle of deviation, θ, from the x-axis (Fig. 12). This set of measurements was used for the purpose of defining mathematically the pre-existing bend in the rod. To connect mathematically two bent rods, the coordinates of the individual rods were mapped into a global coordinate system with the z-axis passing through the endpoints rather than through the pins (Fig. 13). The model of the two rods was then ready to be solved numerically to determine the final deflection under load. The details and

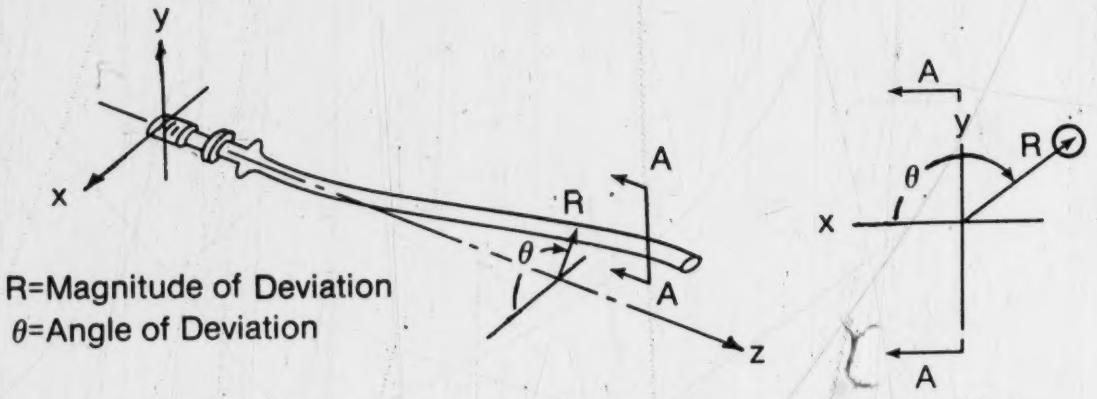

Fig. 12. Angle & Magnitude of Deviation at a Cross Section of Rod

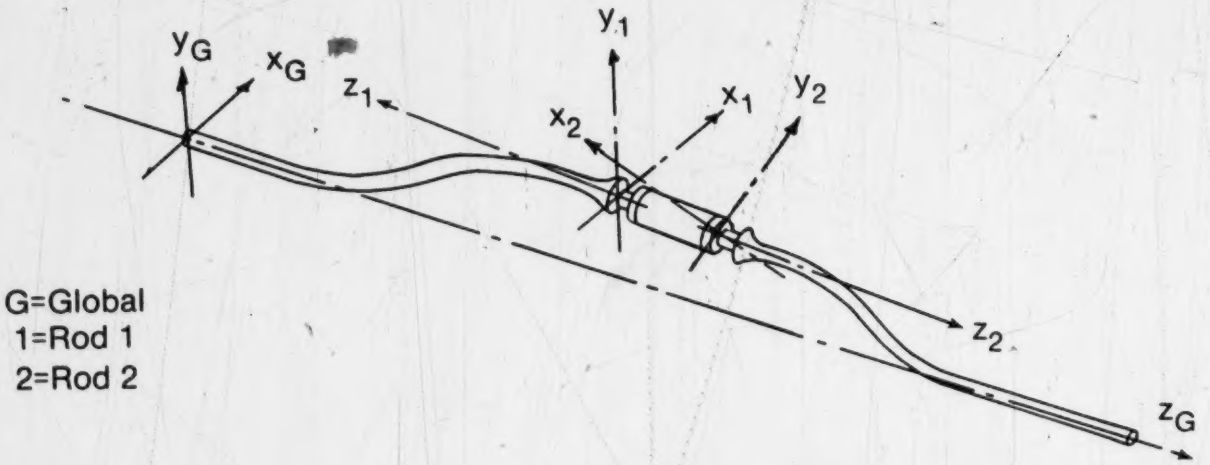

Fig. 13. Mapping of Coordinates of Measured Rods to a Global Coordinate System for Solution

program listings for the transformations are included in Appendix 4.

4.3.2 Measuring Procedure

To measure a rod end, it was first screwed into a coupling that had been previously centred in a lathe chuck (Fig. 14). Subsequently, the rod was rotated about the centre line so that the deviation could be measured at each location for a series of points along the z-axis.

Difficulties arose, though, because the procedure required a high level of accuracy; even small amounts of bend can cause significant bending stresses. Attempts at making accurate measurements were confounded by two factors. First, the location of the centroid at each cross section could not be assumed because the cross sections were asymmetrical as a result of manufacturing imperfections. Since the measurements could only be made at the outer surface of the rod, the asymmetry masked the actual magnitude of the deviation, R, of the centroid from the centre line (Fig. 15). Secondly, the angle of the deviation, θ, from the x-axis was difficult to determine in a single measurement.

The answer to both problems was to determine the vertical deviation, R_i, of the rod from the centre line for a number of rotation angles, α_i, of the rod. The parameters R and θ for a given cross section could then be obtained by using a least squares fit procedure with the vertical

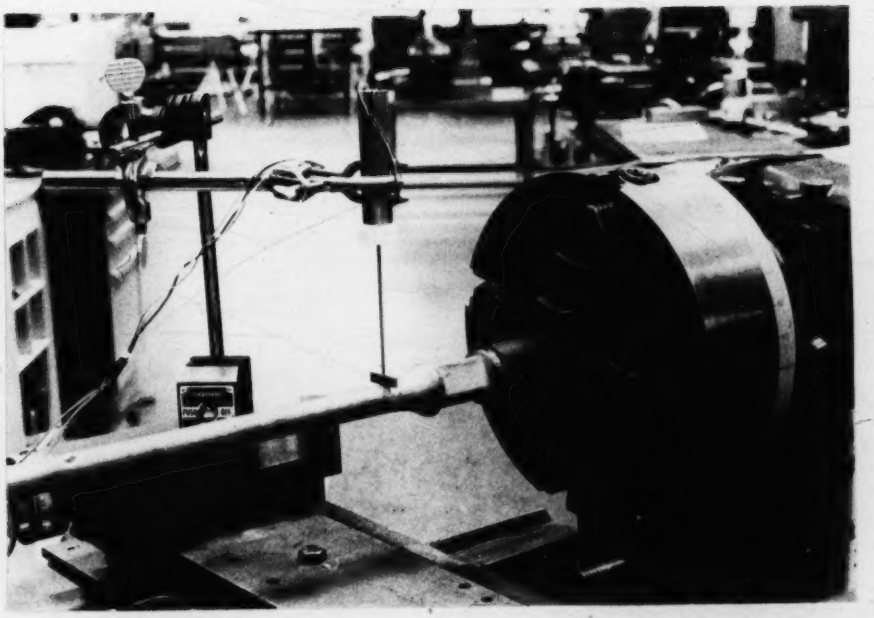

Fig. 14. Rod and Coupling Mounted in Lathe for Measuring Deviation

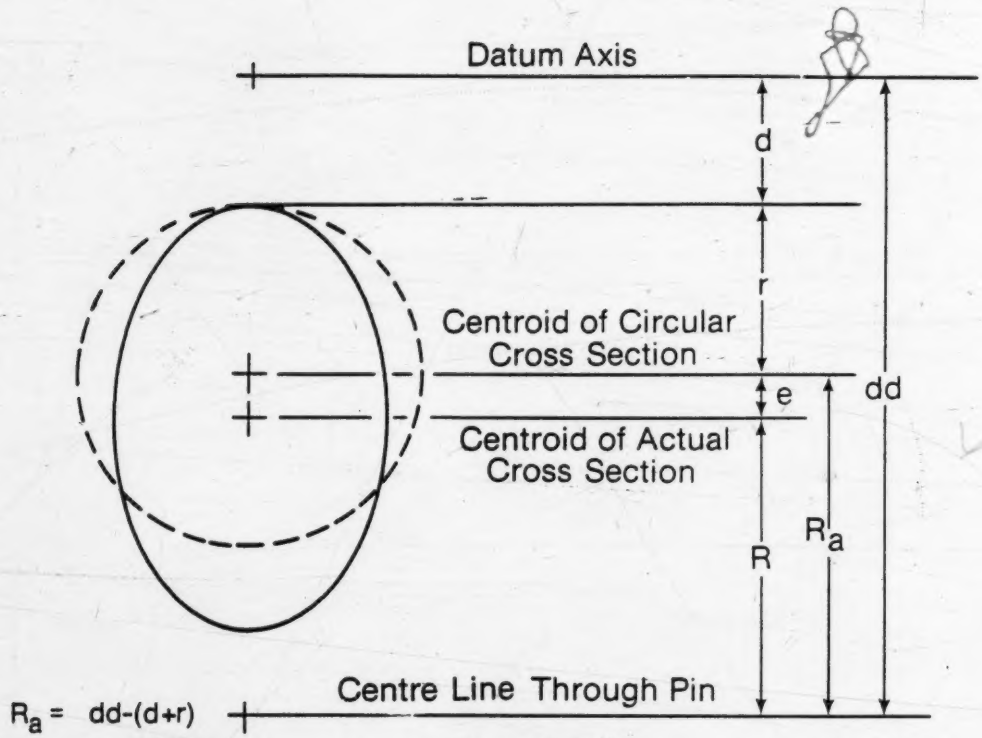

R_a = dd-(d+r)

where

R_a = assumed deviation
dd = datum distance
r = rod radius
d = measured distance
R = true deviation
e = error

Fig. 15. Measurement Error Created by a Non-Circular Cross Section

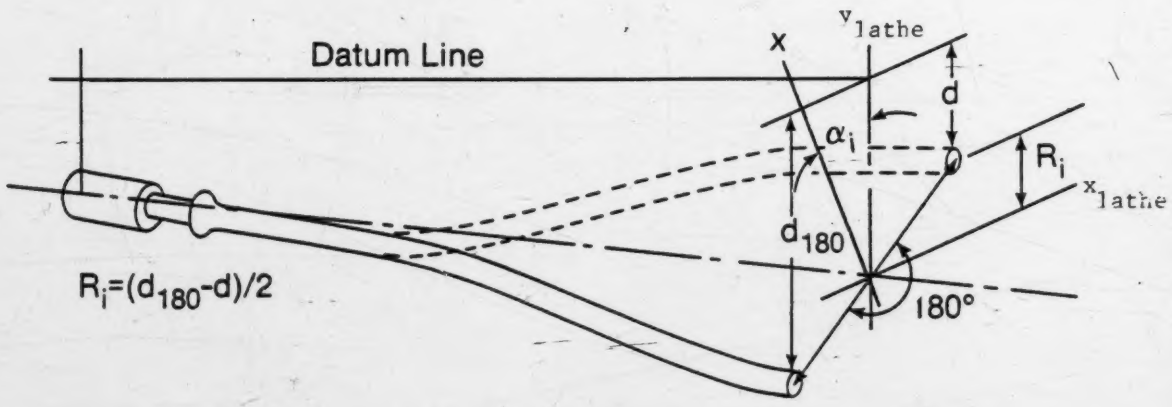

Fig. 16. Finding the Vertical Deviation (R_i) for a Rotation angle (α_i)

deviation data(Appendix 3). The technique resulted in an approximation of the true deviation of the centroid as long as the asymmetry of the cross section was small. To determine R_i for each α_i, the vertical deflection of the rod from a datum line was measured first at α_i and then at a rotation 180 degrees from α_i (Fig. 16). By doing this, errors due to bending deflections and errors due to crooked datum lines were eliminated.

In the actual rod measurements, R_i was determined at six different α_i requiring a total of twelve measurements at each location along the rod axis. The parameters R and θ were then determined using the least squares analysis, and the whole process was repeated for each of the thirty-two locations along the rod length. The measurements were done with a linear voltage displacement transducer (LVDT) hooked up to an analog to digital data acquisition system (Fig. 17) which also took care of the least squares analysis. At a 95% confidence level, the procedure was accurate to ±.001 in.(±0.03 mm) in measuring R and ± 4 degrees (at R=.008 in.) in measuring θ (The accuracy was evaluated by comparing the procedure to a manual method which used a dial gauge for measuring R_i at eighteen different α_i for each cross section).

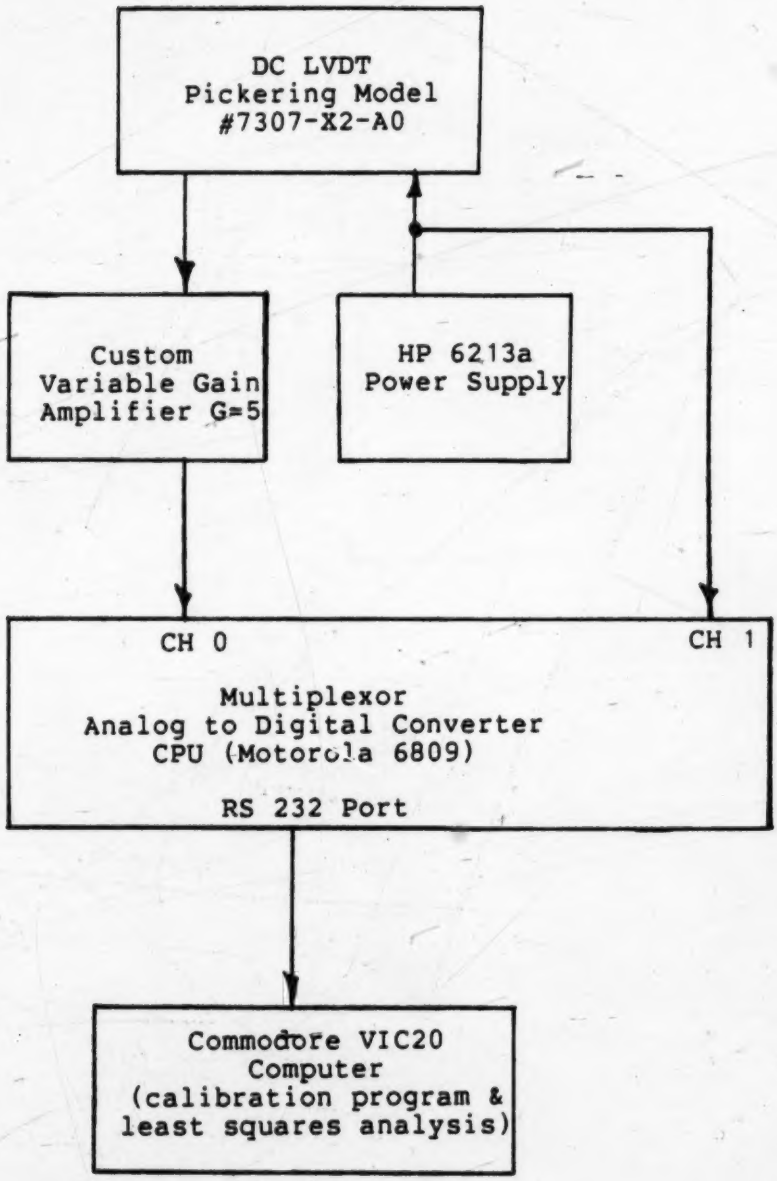

Fig. 17. Schematic of Data Acquisition System

5. Experimental Verification of Model

5.1 Experimental Procedure

The numerical model developed in Chapter IV was confirmed by comparing the strains predicted by the model for three pairs of connected rods with the strains actually measured by strain gauges. The rod ends used in the experimental verification were selected from a group of ten rod ends that had been made by cutting six ft(1760 mm) sucker rods in half. The sucker rods were selected at random from a single batch of 3/4 in.(19 mm) quench and tempered grade C sucker rods that were part of the normal stock at a manufacturing plant.

The sample of rod ends was first measured and analysed using the techniques discussed in Chapter IV. The rod end designated 4a [1] was found to be the straightest and was selected to be used as a common connection rod for calibrating purposes. Two strain gauges, 180 degrees apart, were mounted on the rod 9 in.(23 mm) from the cut end for measuring the nominal axial strains. Three rod ends were selected for testing to compare the predicted bending strains with the actual bending strains: rod 5a, which had the highest predicted bending strain; rod 2a, which had high predicted bending strains though the bend was only detectable by detailed measurement; and rod 3a, which was randomly selected from the remaining rod ends. Four gauges

---

[1] The rods were arbitrarily numbered one to five and their ends labeled "a" and "b" for identification purposes.

were mounted on the test rod ends at the cross section predicted to have the largest bending stresses. For all three rod ends, this location was 3 3/4 in.(95 mm) from the shoulder; at this point, the rod narrows to its nominal diameter. The gauges were spaced 90 degrees apart around the circumference.

For each test, the selected rod end was connected to the common calibration rod end with a standard coupling. The joint was made up using the circumferential displacement method (API, 73) and the relative degree of rotation between the rod ends was measured. Then the rod pair was mounted into a Tinius Olsen tensile testing machine and the gauges were zeroed (Fig. 18). To properly simulate the type of loading found in a rod string, bending moments at the grips of the testing machine were minimized by using a greased hemispherical ball and socket connection (Fig. 19). The rods were then loaded to 15000 lb(66.9 KN) while recording the strains at 1000 lb(4.46 KN) increments (Table 1).

5.2 Experimental Results

The experimental results were in reasonably good agreement with the numerical model especially for loads in the 5000 lb(22.3 KN) to 15000 lb(66.9 KN) range (Figs. 20,21,22). In these figures, the strain ratio * is plotted as a function of the nominal axial stress determined by

---

*The strain ratio is the ratio of bending strain to axial strain and is equal to the DB if the modulus of elasticity is constant.

Fig. 18. Rods Mounted in Tensile Testing Machine

Fig. 19. Ball and Socket Connection for Mounting Rods

Rod Connection	Load kips(KN)	$\mu\epsilon_{axial}$ Measured	$\mu\epsilon_{bending}$ Measured	$\mu\epsilon_{bending}$ Predicted
4a 2a	1 (4.5)	79	130	78
	2 (8.9)	156	176	129
	3 (13.4)	232	208	162
	4 (17.8)	314	233	193
	5 (22.3)	392	254	222
	6 (26.8)	468	263	242
	7 (31.2)	545	281	261
	8 (35.7)	623	298	280
	9 (40.1)	703	314	301
	10 (44.6)	783	329	317
	11 (49.0)	862	344	330
	12 (53.5)	944	345	347
	13 (58.0)	1019	355	356
	14 (62.4)	1097	365	374
	15 (66.9)	1175	375	385
4a 3a	1 (4.5)	81	57	76
	2 (8.9)	159	102	125
	3 (13.4)	233	139	159
	4 (17.8)	313	172	193
	5 (22.3)	391	201	222
	6 (26.8)	469	227	247
	7 (31.2)	546	251	270
	8 (35.7)	625	274	293
	9 (40.1)	704	296	314
	10 (44.6)	787	317	333
	11 (49.0)	864	336	353
	12 (53.5)	926	354	363
	13 (58.0)	1017	371	387
	14 (62.4)	1096	389	403
	15 (66.9)	1175	402	419
4a 5a	1 (4.5)	77	123	130
	2 (8.9)	155	205	212
	3 (13.4)	231	267	268
	4 (17.8)	315	326	323
	5 (22.3)	390	367	360
	6 (26.8)	469	407	397
	7 (31.2)	551	445	433
	8 (35.7)	621	476	456
	9 (40.1)	705	509	487
	10 (44.6)	783	539	515
	11 (49.0)	859	586	542
	12 (53.5)	940	593	566
	13 (58.0)	1020	619	594
	14 (62.4)	1096	645	614
	15 (66.9)	1178	675	638

Table 1. Experimental vs. Predicted Strains

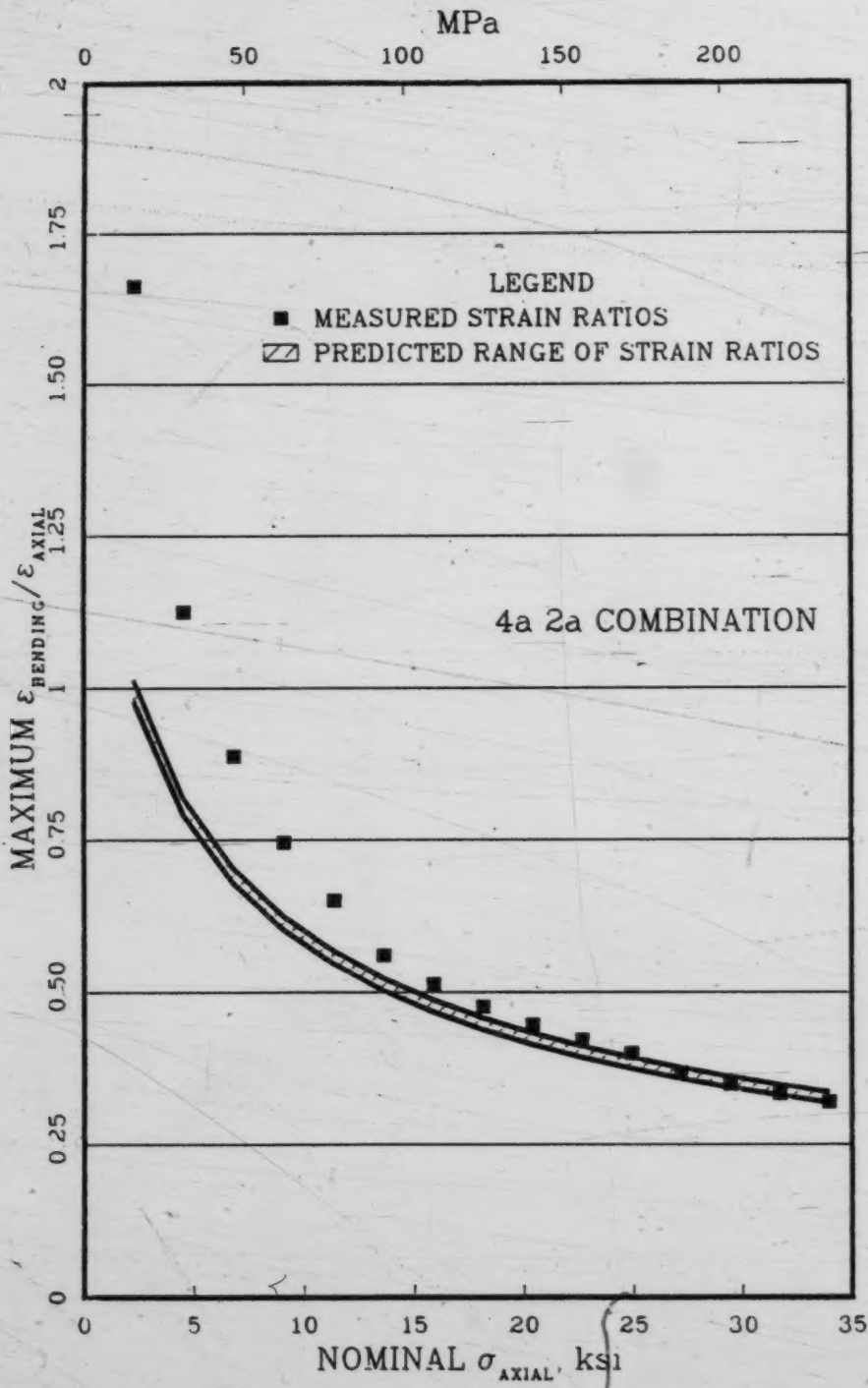

Fig. 20. Comparison of Numerical Solution to Experimental Measurements - 4a 2a Combination

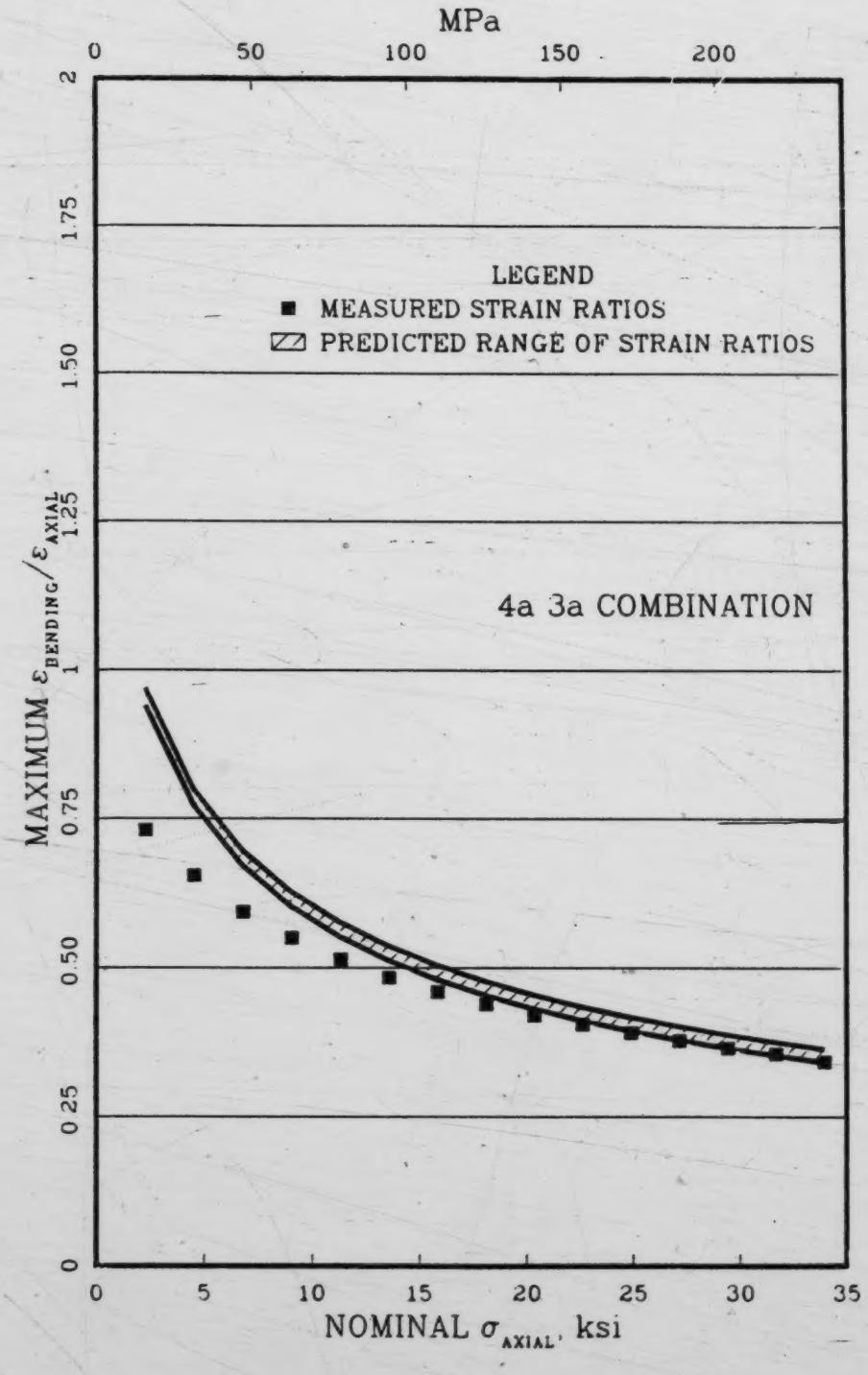

Fig. 21. Comparison of Numerical Solution to Experimental Measurements - 4a 3a Combination

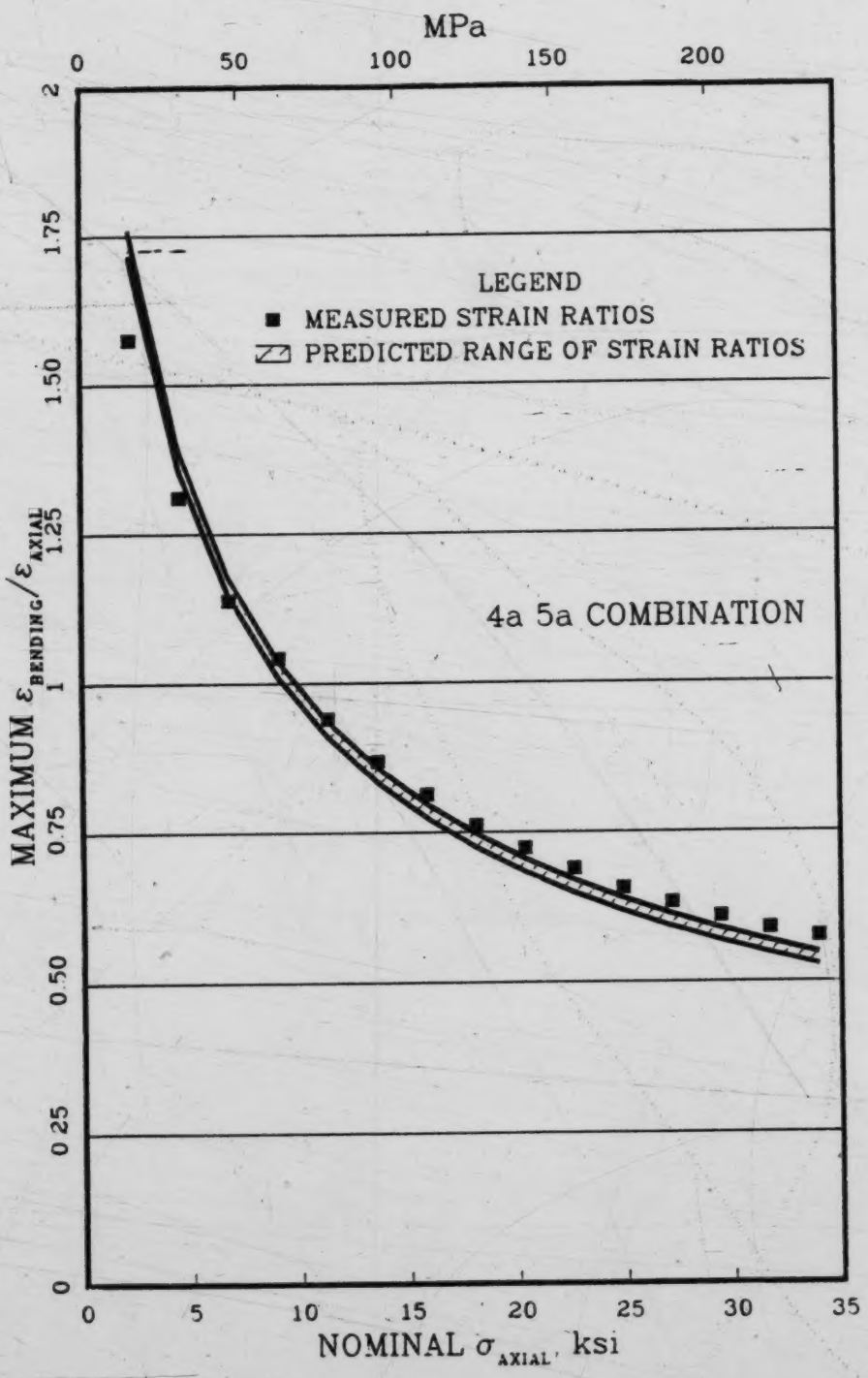

Fig. 22. Comparison of Numerical Solution to Experimental Measurements - 4a 5a Combination

dividing the applied load by the nominal cross sectional area. The predicted strain ratio is shown as a 95% certainty range to account for variation resulting from experimental error in measuring the pre-existing bends. The deviation of the measured strain ratio from the predicted value for small loads can be partly explained by the increasing importance of absolute measurement errors at low strains. If the absolute size of the denominator and numerator is small, small absolute errors can cause large errors in the derived ratio. Also, small moments that may have been present at the grips of the testing machine would have been more noticeable at small loads thereby exerting a greater influence on the observed bending strains. In Fig. 22, the experimental results follow the predicted values closely at low loads but show a trend to be slightly larger at the higher loads. This suggests that there may be an additional factor causing stresses that is not accounted for in the numerical model.

For practical purposes in predicting stresses in the range of loads that are typical for actual conditions, the mathematical model developed works quite satisfactorily. In Chapter VI, the model is used to evaluate the bending stresses that could arise in the sample of rods that was obtained from one manufacturer.

6. Analysis and Discussion of Results

6.1 Introduction

As described in Chapter V, the rod sample selected for analysis consisted of five 6 ft(1760 mm) 3/4 in.(19 mm) pony rods which were cut in half to create ten rod ends. In turn, the ten rod ends represented forty-five possible rod connection pairs, each of which could be connected at a multitude of twist angles. Therefore, the sample allowed a large number of different rod connections to be analysed by the computer model described in Chapter IV. The analysis was used to examine both the details of stresses occurring in individual rod combinations and the overall distribution of stresses occurring throughout the possible range of rod combinations. The intent was three-fold: first, to determine the type of stresses that could arise in non-straight rods; second, to determine to what extent bending stresses may be a problem; and third, to examine current standards and possible replacement standards for measuring and defining straightness.

The particular sample used in the analysis was limited because of the sample's small size and its use of 6 ft(1760 mm) pony rods instead of the standard 25 ft(7600 mm) rods. Since the methods of rod manufacture are basically the same for all sizes and grades of sucker rods, the sample is still useful for indicating the magnitude and distribution of bending stresses that can arise near the end of sucker rods

manufactured by current methods.

6.2 Analysis of Selected Rods

6.2.1 Stress Distribution Along Rod

The predicted stresses occurring in the three rod combinations for which stresses were experimentally measured in Chapter V are plotted in Figures 23, 24, and 25. Both the maximum bending stress and the maximum total stress throughout the length of the connected rods for a 15000 lb(66.9 KN) axial load are presented in the figures. In all the combinations studied, the maximum bending stress occurred at the point where the upset forged section reduces to the nominal diameter. As noted before, this is the location where a significant number of failures have occurred. The bending stresses drop to insignificant values approximately 10 in.(254 mm) from this point of maximum stress. From Figure 25 it can be seen that even a straight rod (4a) can have significant bending stresses when connected to a bent rod.

6.2.2 Factors Affecting the Bending Stress

For any given non-straight rod end, the bending stress will be a complex function of both the axial loading and the geometry of the bend in the other rod of the connection. These two factors make it difficult to assign a single value that will measure the straightness of a non-straight rod

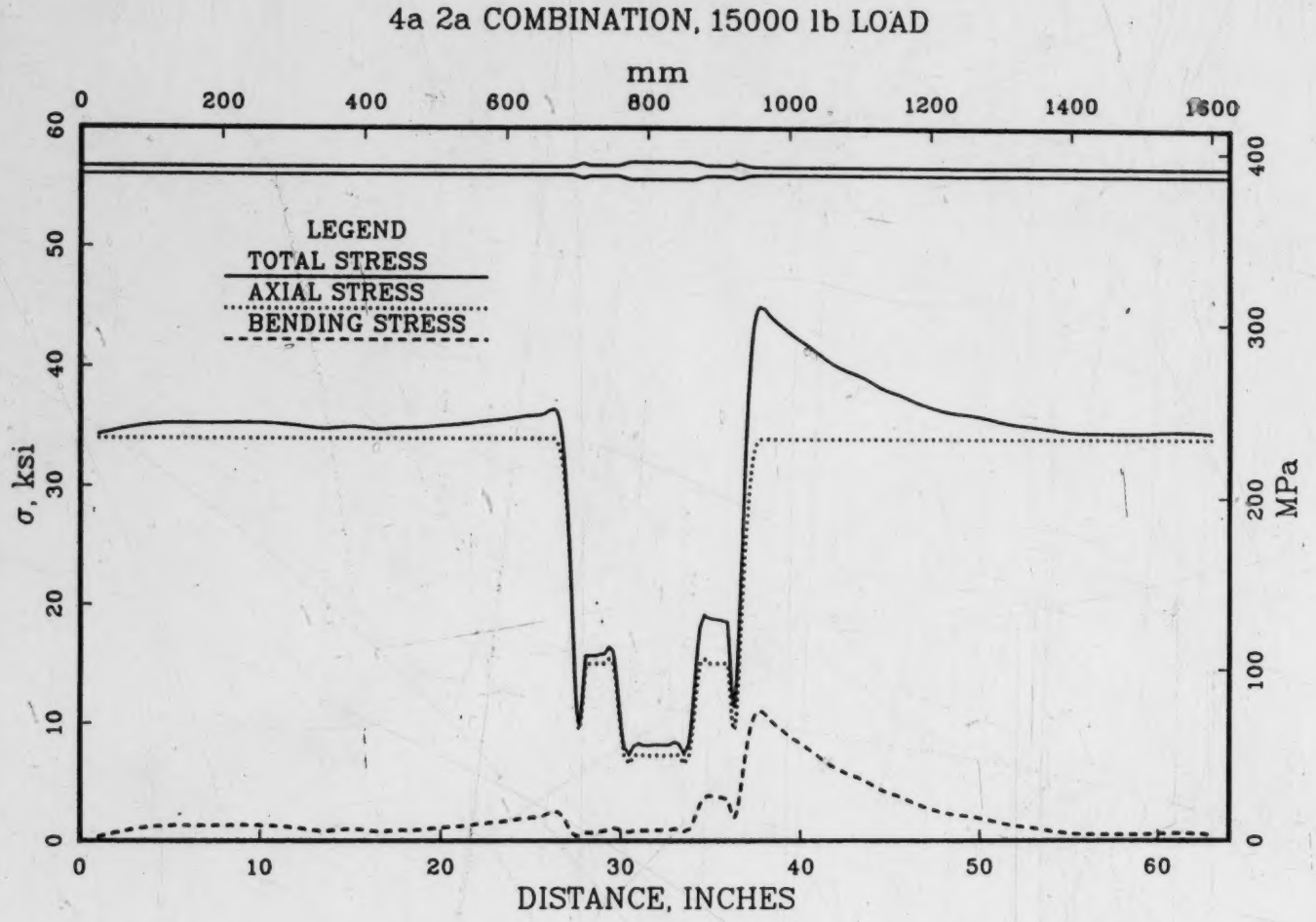

Fig. 23. Stress Distribution Along Length of Connected Rods - 4a 2a Combination

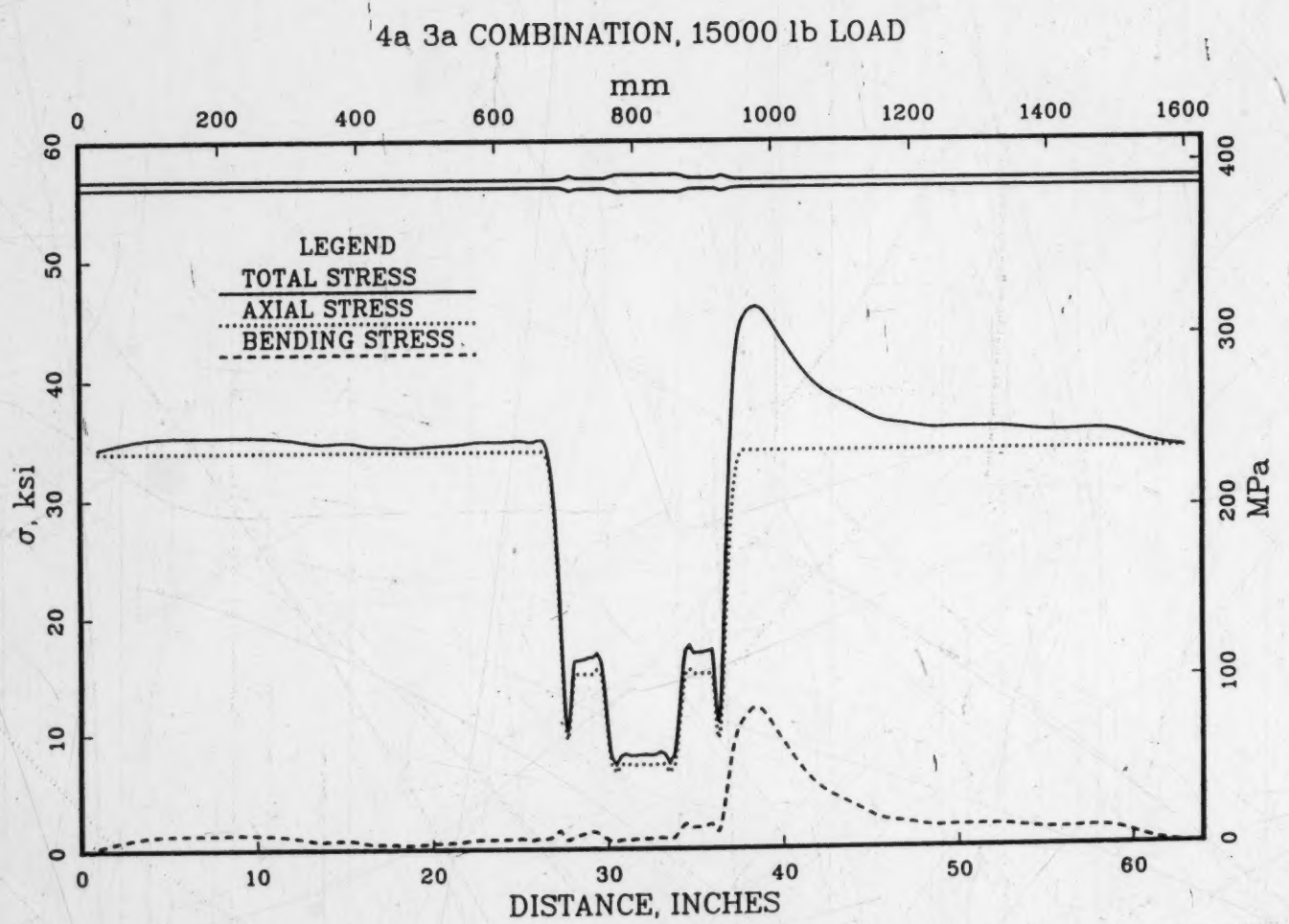

Fig. 24. Stress Distribution Along Length of Connected Rods - 4a 3a Combination

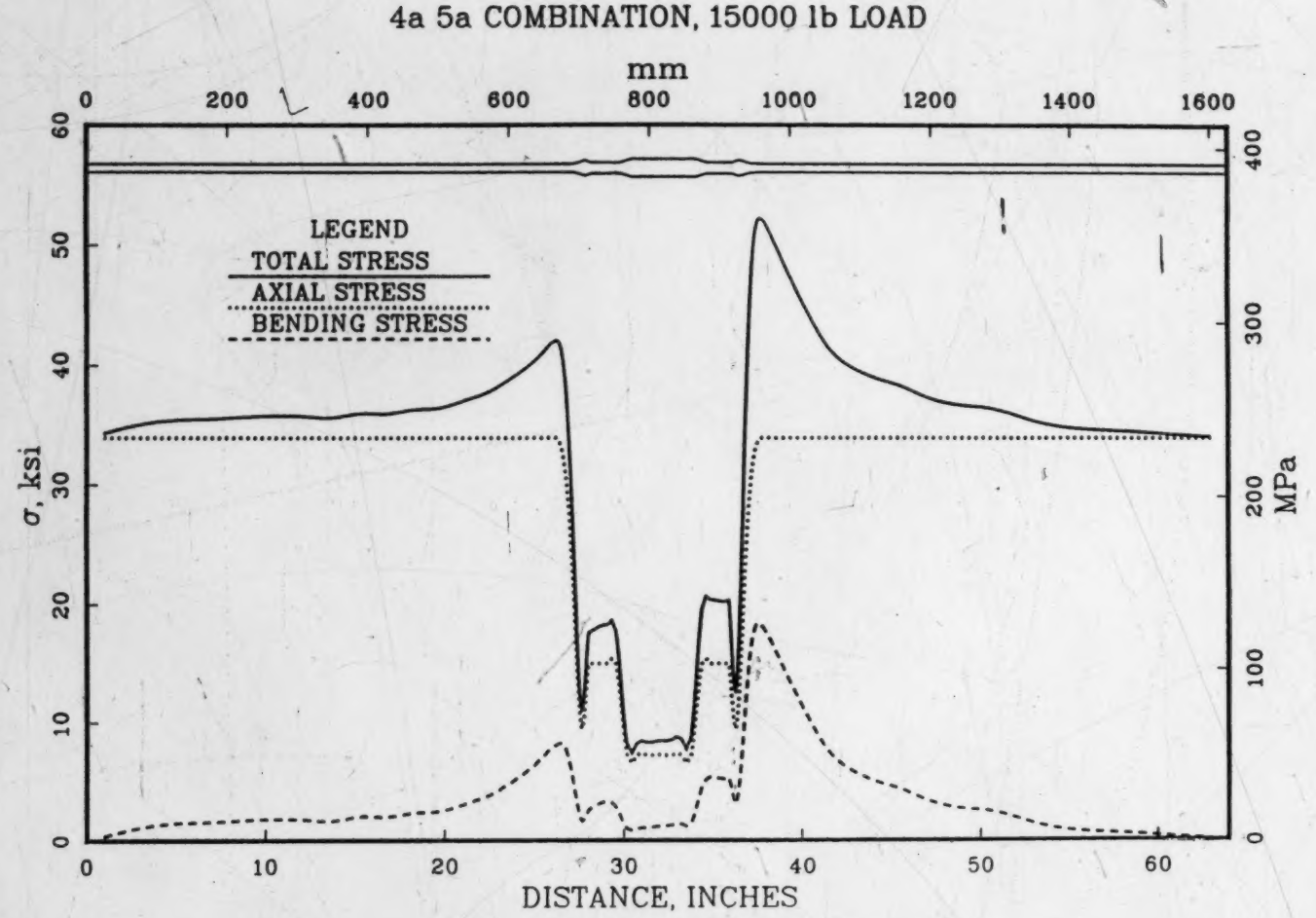

Fig. 25. Stress Distribution Along Length of Connected Rods - 4a 5a Combination

end. As will be shown, the second factor concerning the bend in the other rod of the connection is more difficult to handle than the effect of axial loading.

When an axial load is applied to a given set of connected rods, the pre-existing bend will tend to straighten out thereby decreasing the DB. The analytical solution for a sharply bent bar (Chapter IV) shows that the DB is inversely proportional to the square root of the axial stress. Though this is not true in the general case of a non-straight rod end, the relation gives a reasonable DB approximation (± 10%) for axial stresses ranging from 10 ksi to 34 ksi (70 MPa to 235 MPa) if the DB is originally calculated for an axial stress of 34 ksi(235 MPa). The DB for a different axial stress becomes

$$DB = DB_{34}(34 \text{ ksi}/\sigma_{axial})^{1/2}.$$

Therefore the DB_{34} (dimensionless bending stress for an axial stress of 34 ksi) is useful as a measure of the straightness of a given rod connection.

The main problem arises when one attempts to assign a single measure of straightness to an individual rod end (as opposed to a particular rod connection) without considering the other rod in the connection. In Fig. 26, a frequency plot shows the wide range in DB_{34} (0.4-0.7) that occurs in a single rod as a result of connecting the rod to different rods at a number of twist angles. Even when a given combination of two rods is connected, the twist angle

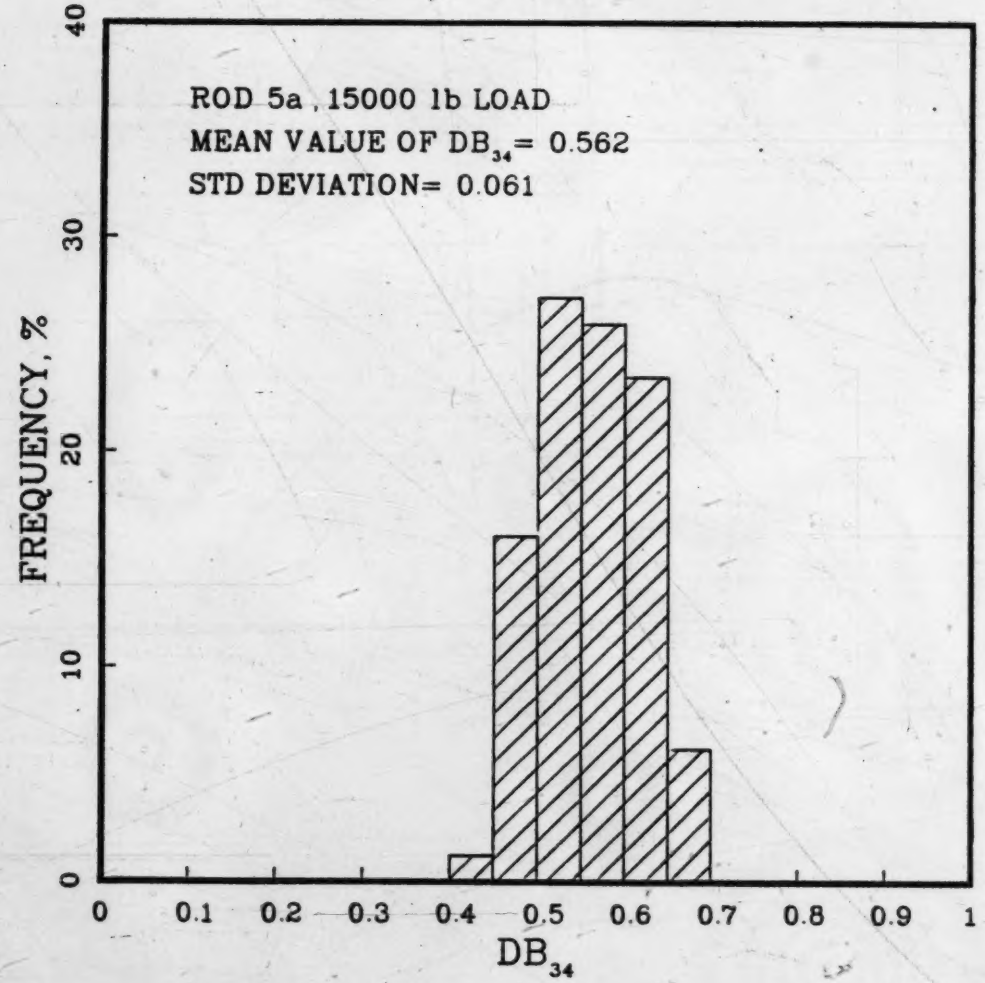

Fig. 26. Range of DB_{34} for Rod 5a

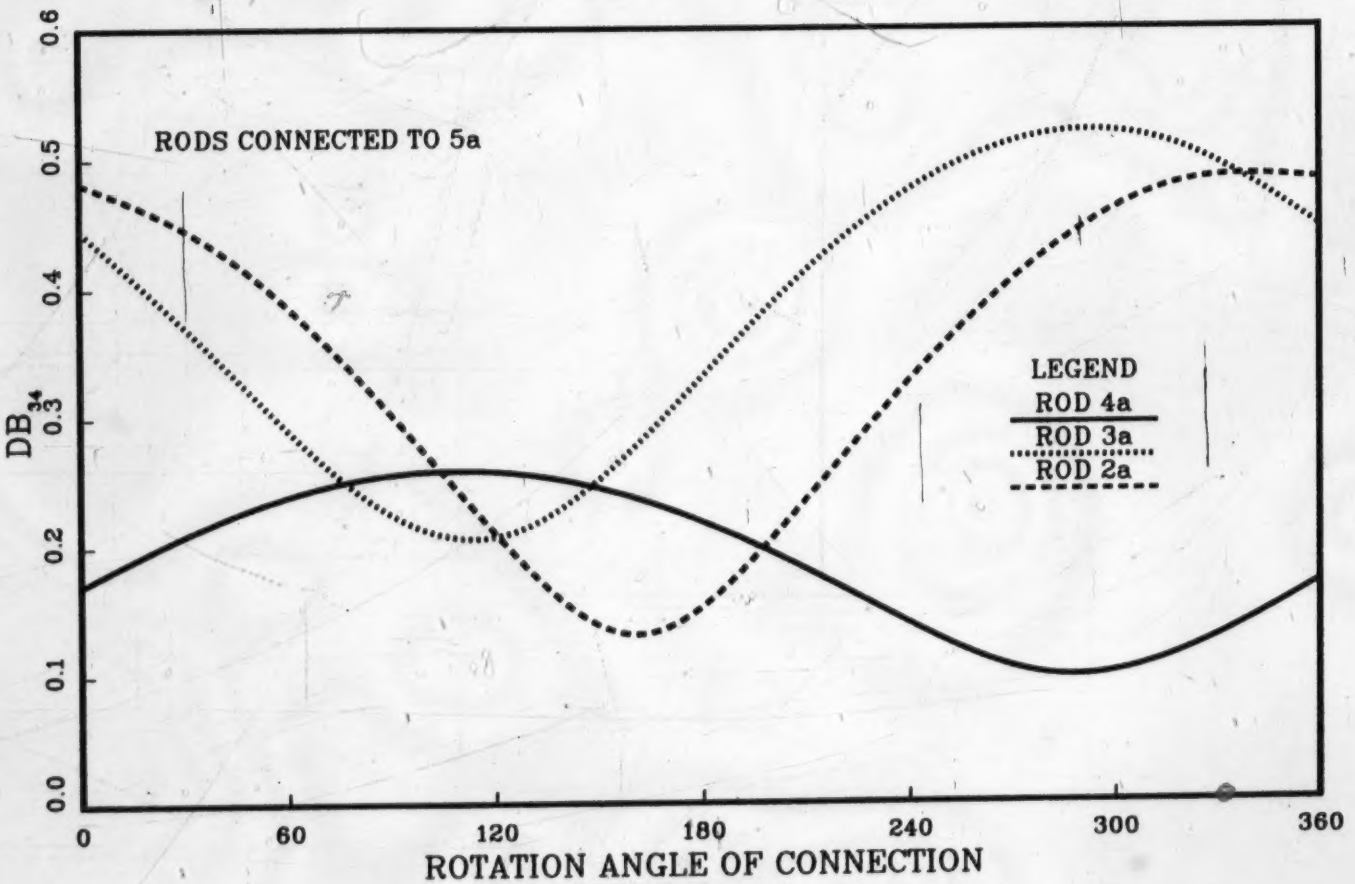

Fig. 27. Variation of DB_{34} due to Variation of Twist Angle of Connection

of the connection can also affect the DB_{34} (Fig. 27). The DB_{34} that occurs when the rod end is connected to a straight rod can be used as a measure of straightness, but this will underestimate the DB_{34} that may occur in actual use (Fig. 26). Both from the perspective of design and from the perspective of manufacturing standards, measures of straightness should consider a particular rod in context with other rods from the same batch.

6.3 Analysis of the Overall Sample

6.3.1 Distribution of Bending Stresses in the Sample

An interesting finding from the computer analysis was the extent to which stresses were increased by small bends at the rod end. In Fig. 28 a frequency distribution is used to illustrate the range in DB_{34} that would be expected in connections made with rods from the sample. The distribution was constructed by analysing each of the possible forty-five rod-pair combinations at twelve different twist angles of connection. The values of DB_{34} extended up to 0.68 with a mean value of 0.29, yet all the rods in the sample passed current API standards on rod straightness. In a rod string loaded to a nominal maximum stress of 34 ksi(235 MPa), a connection with an DB of 0.68 would be loaded to a total stress of 57 ksi(390 MPa).

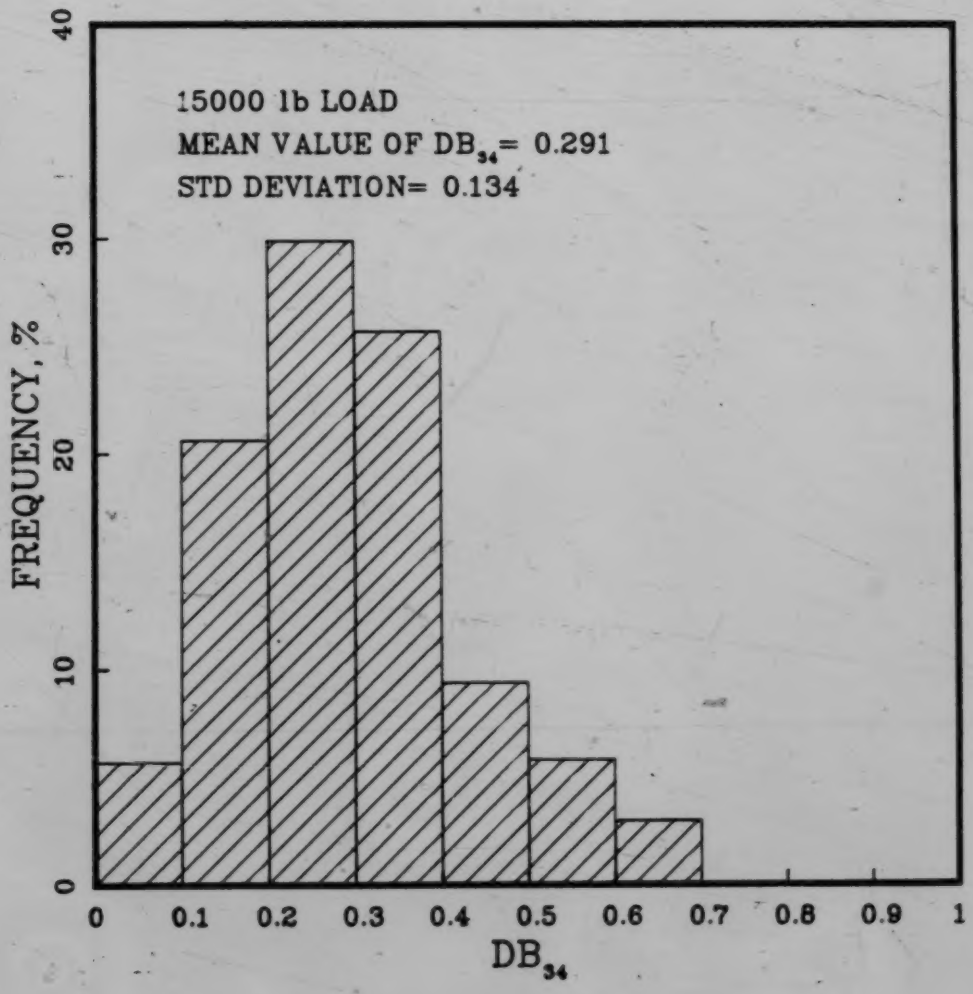

Fig. 28. DB_{34} Frequency Plot for Rod Connections Made from Rods in Sample

6.3.2 Limitations of Current Standards

Based on the above discussion, it would appear that current API standards on rod end straightness (API Spec 11B, Sec 9.2.2, May 82) are not stringent enough. Yet tightening the current standard or making simple modifications to the measurement procedure would not correct the situation because of two basic problems.

The first problem with the API standard is also common to any standard that would define straightness based on the geometry of an isolated rod end. As discussed previously, the DB_{34} is significantly affected by the rod ends to which the rod end in question is connected. Therefore to have meaning, a standard must at some stage consider the isolated rod end as part of a group of rods. Nonetheless, any standard still has to begin by assigning some measure of straightness to the individual rod ends and this is where the API standard has its second and most significant problem.

In the API method, a rod is first centred in a lathe eighteen inches(457 mm) from the rod shoulder. The chuck is then rotated through 360 degrees while a dial gauge is utilized to measure the deviation or total indicator runout (TIR) at the shoulder. The TIR is used as a measure of straightness and is limited to .200 in.(5.1 mm). In Figure 29, the relationship between the DB_{34} ' and the TIR for each of the ten rod ends in the sample is plotted. As can be

---

'The DB_{34} is determined, in this case, by assuming the rod end in question is connected to a straight rod end.

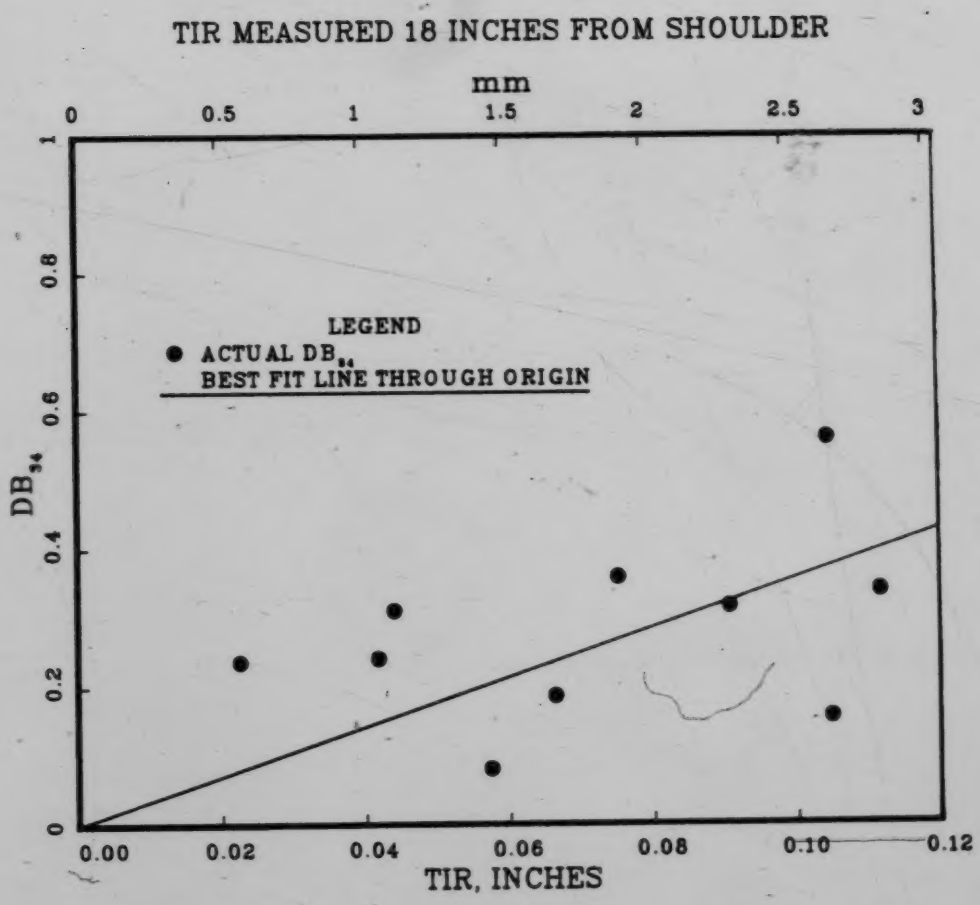

Fig. 29. Comparison of TIR Measured by API Methods to DB_{34}

seen from the figure, the correlation between the TIR and the DB_{34} is poor. As a measure of straightness, the TIR does not work because it fails to correlate the bend with the resulting bending stresses.

After considering that the highest bending stresses occurred close to the upset bead, a modification of the API procedure was tried in which the rod was centred in a lathe four in.(102 mm) from the rod shoulder. Though the correlation between the TIR and DB_{34} is better when using the modified technique (Fig. 30), the method is still ineffective for screening the "crooked" rods from the "straight" rods due to the large scatter of the DB_{34} values for small TIR values.

In summary, the assumptions, that TIR can be used as a measure of straightness and that straightness can be measured in isolation from other rod ends, are simplifications that do not adequately account for the complexity of the bends occurring in the rod ends.

6.3.3 Evaluating Rod End Straightness

One approach to the problem of rod end straightness is to eliminate the standard completely and replace it with an evaluation report detailing the expected stresses for a given batch of rods under different axial loads. This type of approach would also allow the manufacturers to better match existing and future capabilities for rod end straightness with the producers' requirements for

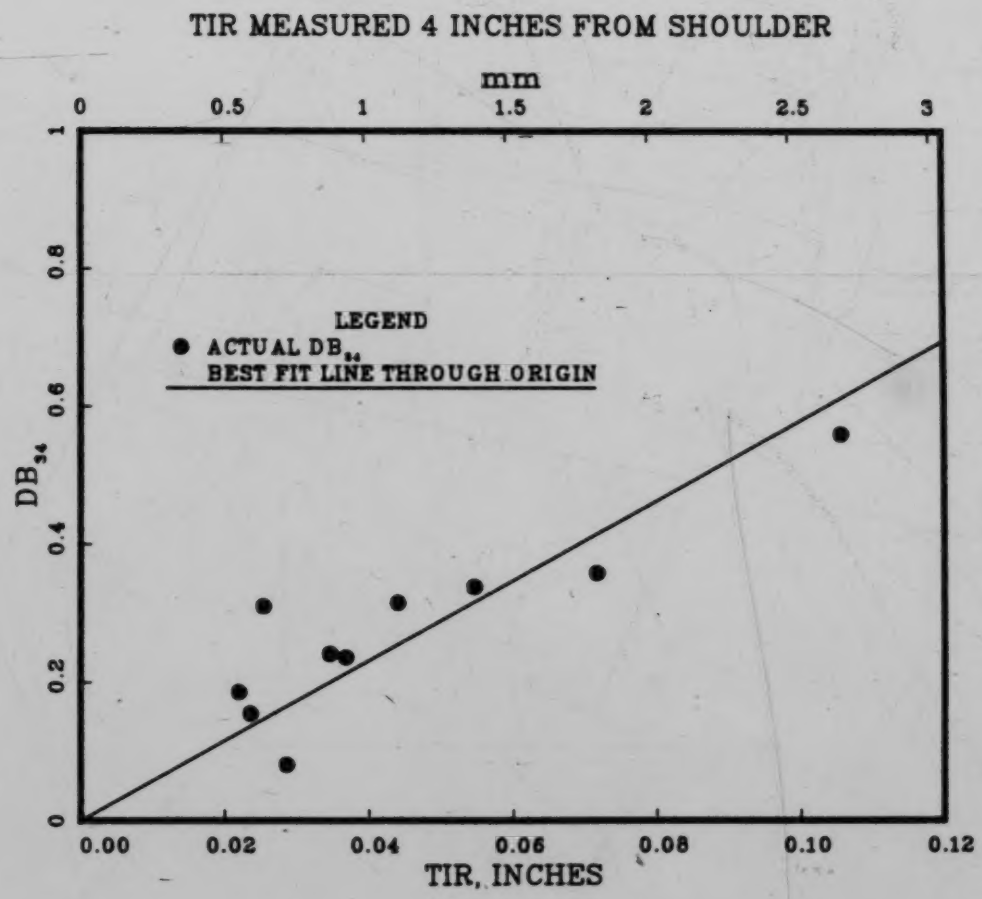

Fig. 30. Comparison of TIR Measured at Four Inches to DB_{34}

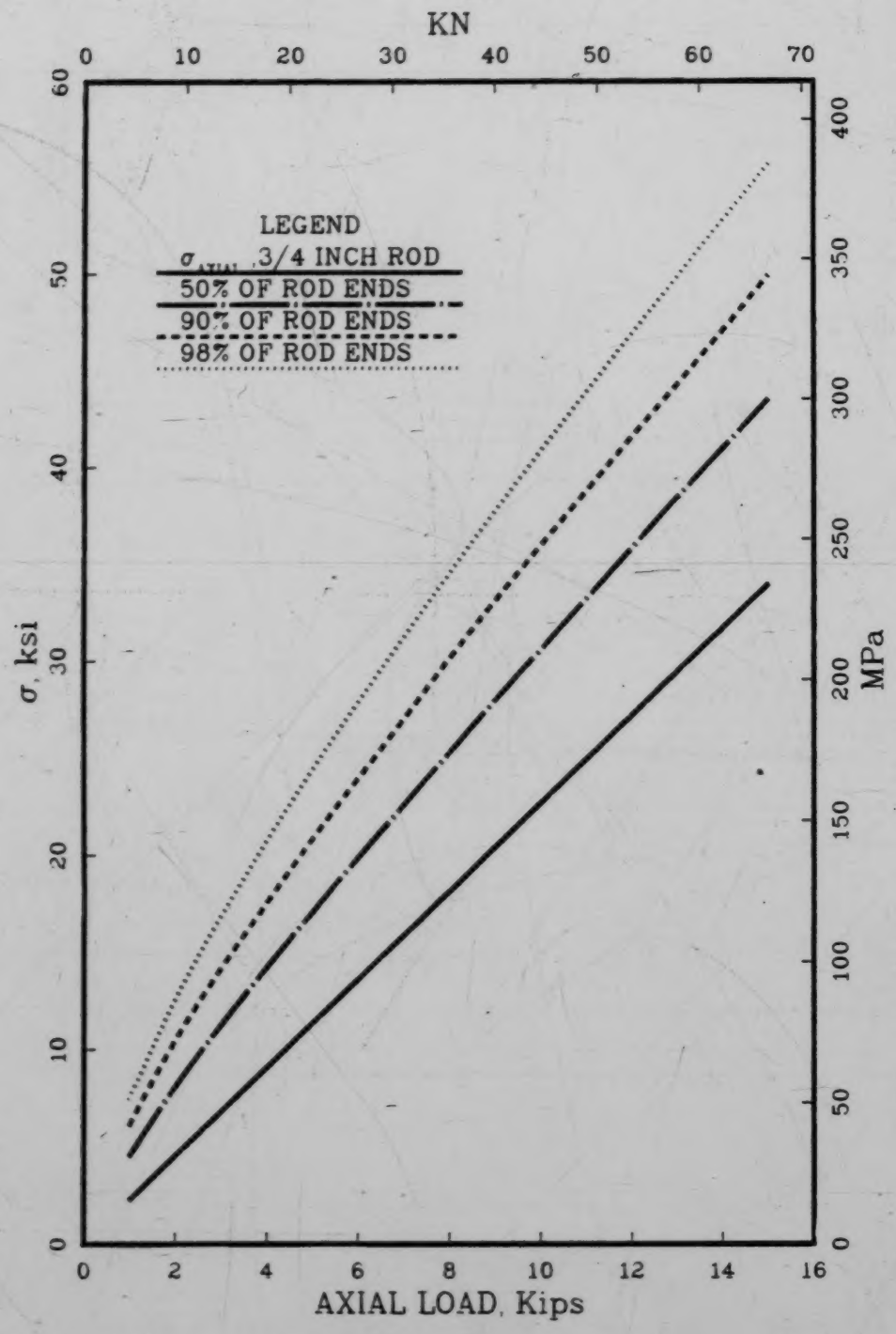

Fig. 31. Design Chart for Upper-Limit Stresses in Rod Sample

load carrying capacity. One possibility for a design and evaluation chart is presented in Fig. 31. In the chart, based on the sample, upper limit curves of the maximum stress as a function of the applied axial load are plotted. The curves represent the upper limit on the maximum stress for a given percentage of rod connections in the sample. For example, the 90% curve represents the upper limit on stresses for 90% of the rod connections; only 10% of the rod connections will have stresses higher than the curve.

From the perspective of design, the 98% curve is the most important because it approximates the average maximum stress which can be expected to occur at some point in a typical rod string made up with rods from the sample. The empirical relationship between the 98% curve and the average maximum stress was found by using a monte carlo simulation technique in which 300 rod strings[10] were modeled numerically using random rod connections selected from the sample studied. With a maximum load of 15 kips(66.9 KN), the average maximum stress was found to be 54 ksi(370 MPa) with a standard deviation of 8 ksi(55 MPa). This corresponds closely to the value of 55.5 ksi(382 MPa) predicted by the 98% curve.

---

[10]The rod string model was constructed of 400 rods with a total of 133 - 3/4 inch(19 mm) rods in the top section.

7. Conclusions

The combination of the measurement technique and the numerical model can be concluded to be an effective and accurate method for determining the bending stresses that can arise in bent rod ends.

The dimensionless bending stress (DB), defined as the bending stress divided by the axial stress, was a useful concept for evaluating the relative importance of bending stresses. The maximum value for the DB occurred where the upset bead narrows to the nominal diameter of the rod. For a given rod end, the DB was a complex function of both the magnitude of the axial load and the geometry of the other rod in the connection.

In the sample that was used, the DB extended up to 0.68 with a mean value of 0.29 for an axial load of 15 kips(66.9 KN). A DB of .68 would result in a total stress of 57 ksi(390 MPa) in a rod string loaded to a nominal maximum stress of 34 ksi(235 MPa). Though the sample cannot be considered to be a representative sample of sucker rods, the sample does illustrate the large bending stresses that can occur in rod ends.

The present API standard on rod end straightness was concluded to be inadequate. The TIR value used by the standard to measure straightness did not correlate with the bending stresses arising in the rod ends.

Bibliography

Amezcua, J., "Comparative Analysis of Pump-off Control Systems for Field Applications," 55th Annual SPE of AIME Fall Technical Conference (Dallas, 9/21-24/80), preprint SPE 9362, 1980.

API Bul. 11L3, *Sucker Rod Pumping System Design Book*, 1st ed., May, 1970.

API RP 11BR, "API Recommended Practice for Care & Handling of Sucker Rods," 5th ed., Mar., 1969.

API RP 11L, "API Recommended Practice for Design Calculations," Feb., 1977.

API Spec. 11B, "API Specification for Sucker Rods," 19th ed., May, 1982.

API Supplement 1 to API RP 11BR, Mar., 1973.

Atkey, J., MacDonald, R., "An Analysis of Corrosion Related Rod-Pumping Equipment Failures," Canadian Region Western Conference of the National Association of Corrosion Engineers (Edmonton, 2/12-14/80), conference paper, 1980.

Atkinson, O., "A Program to Reduce Sucker Rod Failures - West Kansas Operations," *Drilling & Production Practice*, API, 1960, pp.64-67.

Baron, J., "House Mountain Field Sucker Rod Corrosion, a Case History," Canadian Region Western Conference of the National Association of Corrosion Engineers (Edmonton, 2/12-14/80), conference paper, 1980.

Barsom, J., "Fatigue Crack Propagation in Steels of Various Yield Strengths," *Journal of Engineering for Industry*, ASME, v.93, 1971, pp.1190-1196.

Bellow, D., Kumar, A., "Stress Analysis of Bent Sucker Rods," *The Journal of Canadian Petroleum Technology* v.17, n.3, July-Sept., 1978, pp.76-81.

Bellow, D., "Stress & Corrosion Fatigue Experiments on Oil Field Components," Proceedings SESA/SEJA, Hawaii, 1981, pp.647-658.

Bonis, M., Crolet, J., "pH Measured in Aqueous CO_2 Solutions Under High Temperature & Pressure," *Corrosion*, v.39, n.2, Feb., 1983, pp.39-46.

Broek, D., *Elementary Engineering Fracture Mechanics*, Noordhoff International Publishing, Leyden, 1974.

Bucaram, S., Byars, H., Kaplan, M., "Selection, Handling, & Protection of Downhole Materials: A Practical Approach," *Materials Protection & Performance*, v.12, n.9, Sept., 1973, pp.20-26.

Chastain, J., "Proper Care Extends Sucker Rod Life," *The Oil & Gas Journal*, v.75, n.8, Feb. 21, 1977; p.88.

Coberly, C., "Problems of Modern Deep Well Pumping," *The Oil & Gas Journal*, May 12, 1938, pp.126-137.

Copson, H., "Literature Survey on Corrosion in Neutral Unaerated Oil Well Brines," *Corrosion*, v.7, n.4, Apr., 1951, pp.123-127.

Couch, S., "Corrosion vs. Scale - Identifying Downhole Deposits," Kansas University and Western Kansas Chapter API Kansas Oil Lifting Short Course (Great Bend, 3/11-12/81), 1981.

Crevolin, J., *Epoxy Coating of Steel Sucker Rods*, Caproco Corrosion Prevention Ltd., in-house publication, Edmonton, 1980.

Crosby, B., "Fully Rolled Thread: Breakthrough in Rod Couplings," *Petroleum Engineering*, July, 1970, p.70.

Dale, D., Johnson, D., "Laboratory & Field Endurance Values of Sucker Rod Materials," *Drilling & Production Practice*, API, 1940, pp.209-218.

Detterick, J., Saul III, H., "Utilization of Fiberglass Sucker Rods," *Journal of Petroleum Technology*, Aug., 1980, pp.1339-1344.

Doty, D., Schmidt, Z., "Improved Model for Sucker Rod Pumping," *Society of Petroleum Engineering Journal*, Feb., 1983, pp.33-41.

Duquette, D., "A Review of Aqueous Corrosion Fatigue," *Corrosion Fatigue: Chemistry, Mechanics, & Microstructure*, NACE 2, Univ. of Conn., 1972.

Duquette, D., Laird, C., "Mechanisms of Fatigue Crack Nucleation," *Corrosion Fatigue: Chemistry, Mechanics, & Microstructure*, NACE 2, Univ. of Conn., 1972.

Duquette, D., Ulhig, H., "Effect of Dissolved Oxygen & NaCl on Corrosion Fatigue of 0.18% Carbon Steel," *Transactions of the ASM*, v.61, 1968, pp.449-456.

Duquette, D., Ulhig, H., "The Critical Reaction Rate for Corrosion Fatigue of 0.18% Carbon Steel & the Effect of pH," *Transactions of the ASM*, v.62, 1969, pp.839-845.

Dvoracek, L., "Corrosion Fatigue Testing of Oil Well Sucker Rod," *Materials Protection & Performance*, v.12, n.9, Sept., 1973, pp.16-19.

Eaton, J., "Tests Indicate Sucker Rod Loads May be Reduced," *Drilling & Production Practice*, API, 1935, pp.239-249.

Ewing, R., "Technology of a Long Stroke Pumping Unit," *Oilweek*, Sept. 20, 1971, pp.45-47.

Gibbs, S., Neely, D., "Computer Diagnosis of Down-hole Conditions in Sucker Rod Pumping Wells," *Journal of Petroleum Transactions*, Jan., 1966, pp.91-98.

Gibbs, S., "Predicting the Behavior of Sucker Rod Pumping Systems," *Journal of Petroleum Technology*, July, 1963, pp.769-778.

Gilbert, W., "An Oil Well Pump Dynagraph," *Drilling & Production Practice*, API, 1936, pp.94-115.

Glikman, L., *Corrosion-Mechanical Strength of Metals*, Butterworth & Company Ltd., London, 1962.

Griffin, F., "New API Design Calculations for Sucker Rod Pumping Systems," *Drilling & Production Practice*, API, 1968, pp.220-231.

Gupta, S., "Corrosion Behavior of 1040 Steel 1. Effect of pH & Sulphide Ion Concentrations in Aqueous, Neutral, and Alkaline Solutions," *Corrosion*, v.37, n.11, Nov., 1981, pp.611-616.

Holliman, J., Madrazo, A., "Review of Sucker Rod Pumping Problems South Glenrock Block 'B' Unit Converse County, Wyoming," *Drilling & Production Practice*, API, 1966, pp.175-185.

Hudgins, C., McGlasson, R., Mehdizadeh, P., Rosborough, W., "Hydrogen Sulphide Cracking of Carbon & Alloy Steels (1966)," *H_2S Corrosion in Oil & Gas Production- A Compilation of Classic Papers*, NACE, 1981.

James, M., Smith, G., Wolford, J., *Applied Numerical Methods for Digital Computation*, Harper & Row, New York, 1977.

Jaske, C., Payer, J., Balint, V., *Corrosion Fatigue of Metals in Marine Environments*, Battelle Press, Columbus, Ohio, 1981.

Li, S., "Stress Analysis on a Sucker Rod," *Oil Field Equipment*, v.13, n.4, July, 1984, pp.23-29 (in Chinese).

Makarov, V., Savelev, V., Mukhamadeeva, N., "Causes of Premature Failure of Sucker Rods in the Heat Affected Zone," *Neft. Khoz.*, n.11, Nov., 1981, pp.40-42 (in Russian).

Martin, R., "Diagnosis & Inhibition of Corrosion Fatigue & Oxygen Influenced Corrosion in Oil Wells," *Material Performance*, v.22, n.19, Sept., 1983, pp.33-36.

Martin, R., "Hydrogen Penetration & Damage to Oil Field Steels," *Material Performance*, v.13, n.7, July, 1974, pp.19-23.

Martin, R., "Inhibition of Corrosion Fatigue of Oil Well Sucker Rod Strings," *Material Performance*, v.19, n.6, Jun., 1980, pp.20-23.

Maradudin, A., "Drill Pipe, Casing, Tubing, Sucker Rods: Corrosion Failures & Methods of Combatting Corrosion," *Materials Protection*, v.4, n.12, Dec., 1965, pp.45-51.

McReynolds, R., Vennett, R., "Corrosion Fatigue Testing as a Method of Evaluating Corrosion Inhibitors in Oil Field Environments," *Material Performance*, v.14, n.1, Jan., 1975, pp.23-27.

Mehdizadeh, P., "Effect of Metallurgical Variables on Corrosion of Sucker Rods in Salt Water Containing CO_2 & H_2S," *Material Performance*, v.13, n.6, Jun., 1974, pp.13-16.

Mehdizadeh, P., McGlasson, R., "Effect of Organic Inhibitors on Corrosion Fatigue," *Corrosion*, v.23, n.3, Mar., 1967, pp.65-71.

Midwest Research Institute, "Electric Analog Study of Sucker Rod Pumping Systems," *Drilling & Production Practice*, API, 1968, pp.232-249.

Mills, K., *API Production Bulletin 230*, API, 1943.

NACE MR-01-75, "Sulphide Stress Cracking Resistant Metallic Material for Oil Field Equipment," NACE, Houston, 1975.

NACE TPC Publication 3, *The Role of Bacteria in the Corrosion of Oil Field Equipment*, NACE, Houston, 1976.

Nestle, A., "Corrosion Inhibitors in Petroleum Production Primary Recovery," *Corrosion Inhibitors*, edited by C.C. Nathan, NACE, Houston, 1973, pp.61-75.

Paul,R., *Robot Manipulators: Mathematics, Programming, and Control*, MIT Press, Cambridge, 1981.

Pearson, W., "Corrosion Prevention in Western Kansas (Practical Results of a Planned Program)," *Drilling & Production Practice*, API, 1948, pp.239-246.

Rogers, W., Shellshear, W., "Corrosion of Steel by Oil Well Waste Waters," *Ind. Eng. Chem.*, 29, 160, 1937, pp.160-166.

Shehorn, L., "Corrosion Monitoring on Rod-Pumped Wells Using Linear Polarization Probes," 55th Annual SPE of AIME Fall Technical Conference (Dallas, 9/21-24/80), preprint SPE-9363, 1980.

Shigley,J., *Mechanical Engineering Design*, 3rd edition, McGraw-Hill, U.S.A., 1977.

Shock, D., Sudbury, J., "Prediction of Corrosion in Oil & Gas Wells," *Drilling and Production Practice*, API, 1951, pp.339-348.

Steward, W., "Sucker Rod Failures," *Oil and Gas Journal*, v.71, n.15, Apr. 9, 1973, pp.53-76.

Sucker Rod Handbook (Handbook 282), Bethlehem Steel Co., Lebanon, Pa., 1950.

Swanson, T., Treseder, R., "Factors in Sulphide Corrosion Cracking of High Strength Steels," *H_2S Corrosion in Oil and Gas Production: A Compilation of Classic Papers*, NACE, 1981.

Thompson, M., "Know Your Well Loads," *Oil and Gas Journal*, v.57, n.18, 1959, pp.157-163.

Ulhig, H., Lee, H., "Corrosion Fatigue of Type 4140 High Strength Steel," *Metallurgical Transactions*, v.3, 1972, pp.2949-2957.

Vollmer, L., "The Undercut Sucker Rod Joint," a paper presented at the Symposium on Sucker Rods during the API midyear standardization meeting, Denver, June, 1952.

Wescott, B., "Corrosion Fatigue," *Corrosion Handbook*, edited by Ulhig, John Wiley & Sons Pub., New York, 1948, pp.573-590.

Zaba, J., *Modern Oil Well Pumping*, The Petroleum Publishing Co., Tulsa, 1962.

Appendix 1: API Sucker Rod Grades

Section 2.1 of API Spec. 11B (API, 1982) specifies the requirements for API C, D, and K grade sucker rods and pony rods. The specification does not prevent manufacturers and purchasers from producing or purchasing sucker rods made to different specifications. The three grades are described below.

1. Grade C rods are to be made from a carbon-manganese steel (AISI 1036 or similar) with a min. tensile strength of 90 ksi(620 MPa) and a max. allowable tensile strength of 115 ksi(793 MPa).

2. Grade D rods can be made from any steel (carbon or alloy) which can be heat-treated to a min. tensile strength of 115 ksi(793 MPa) with a max. allowable tensile strength of 140 ksi(965 MPa).

3. Grade K rods are to be made of a nickel and molybdeum steel (AISI 46xx) with a min. tensile strength of 85 ksi(586 MPa) and a max. tensile strength of 115 ksi(793 MPa).

Appendix 2: Sucker Rod Failure Mechanisms

Introduction

Sucker rod failures can be rationally understood if the basic mechanisms of failure are understood. This appendix first examines the basic theory of fatigue failure and the importance of crack initiation in sucker rod failures. This is followed by an investigation of the factors which can lead to sucker rod corrosion. The appendix closes with a literature review of the interaction of the environment with fatigue processes; in particular, corrosion fatigue, pitting attack and hydrogen sulphide cracking are examined.

Fatigue Failure

Theory of Fatigue

Fatigue failure is a cumulative damage mechanism resulting from repeated stress fluctuations. The metal will eventually fail at stresses below those required for static failure. The process can be divided into three stages each of which has a different driving mechanism.

Crack initiation is the first (Stage I) and also the least understood phase of metal fatigue. Since it is a surface phenomenom, surface conditions and the surrounding environment can have strong influences on both the rate and the primary mechanism of crack initiation. In the absence of damaging environments, cyclic stresses cause local plastic

strain reversals on the metal surface. These local plastic strains occur at stresses below the bulk yield stress of the material and result in the initiation of a crack. When corrosive environments or environments containing H_2S are present, crack initiation is only partly understood; in some instances, cyclic stresses may not be required for crack initiation to occur.

The second step (Stage II) of fatigue involves the growth of the initiated crack under an imposed cyclic stress. The stress intensity range at the crack tip is the important parameter in determining the rate of crack propagation (Broek,1974). Both in the presence of high mean stresses or damaging environments, the initial crack size required for the start of Stage II crack growth will be smaller. Also, damaging environments will accelerate Stage II crack propagation. The final stage (Stage III) of fatigue failure occurs when the crack reaches a critical size; sudden failure will occur either by unstable crack propagation or by ductile fracture.

Within the normal range of sucker rod stresses and service life, the two key parameters are the rate of crack initiation and the initial crack size which is required for Stage II propagation to begin. Once Stage II propagation has started, failure will occur in less than 40 days(600 000 cycles) even in non-damaging environments (Fig. I). Clearly once Stage II crack propagation has started, the remaining service life of a rod string is minimal.

Once a crack is present, the growth of the crack can be estimated by empirical formulas that relate Stage II crack growth, da/dn, to the tensile stress intensity at the crack tip, K_I. The calculations for estimating the number of cycles to failure, N, use the Barsom equation (Barsom,1971) for carbon steels which relates the Stage II crack growth to the change in stress intensity, ΔK_I, as follows:

$$da/dn = 3.6*10^{-10}(\Delta K_I)^3 \text{ (ksi}\sqrt{\text{in.}}\text{)}.$$

A reasonable value for ΔK_I can be obtained by considering the crack to be in plane strain in an infinitely deep plate in which

$$\Delta K_I = (\sigma_{max}-\sigma_{min})\sqrt{a\pi} \text{ (Broek,1974)}.$$

Not until the crack length, a, has become comparable to the rod radius does this assumption become invalid. Since this later period of crack growth represents only a small part of the total cycles, the original assumption remains a reasonable approximation.

Using a σ_{max} of 34 ksi(235 MPa) and a σ_{min} of 14 ksi(96 MPa), this expression for ΔK_I can be substituted into the Barsom equation and integrated as follows:

$$62350 \int_{a_i}^{a_f} a^{-3/2} = \int_0^N dn$$

which reduces to

$$N = 124700(a_i^{-1/2} - a_f^{-1/2})$$

where a_i and a_f are the initial cracksize and failure cracksize respectively. Without loss of significant accuracy, a_f can be taken as .75 in.(19 mm) even though ductile failure or, alternatively, unstable crack propagation will have occurred prior to the propagation of the crack through the rod diameter. a_i is determined by taking the $K_{threshold}$ for Stage II crack growth as 10 ksi$\sqrt{\text{in.}}$ (Barsom) giving a_i equal to .03 in.(.75 mm). Substituting these values into the preceding equation gives N equal to 575960 cycles.

In other words, the remaining service life is only about 40 days (10 strokes/minute) once a crack is present.

Fig. I. Calculation of Time to Failure for Stage II Crack Propagation

Empirical Studies

Since crack intitiation mechanisms have yet to be quantified, empirical fatigue data is used for design purposes. The data is plotted on an S-N chart, which is a plot of the amplitude of the stress fluctuation as a function of the number of cycles required to give a 50% chance of failure. For steels cycled in non-damaging environments and in the absence of stress concentrations, the S-N chart shows an endurance limit. Stress amplitudes below this endurance limit will result in an infinite fatigue life. With sucker rod strings, an obvious goal would be to design for stresses below this endurance limit.

The normal design procedure for sucker rods in non-damaging environments is to limit stresses to ranges defined by the API modified Goodman chart (API,1969). For a typical stress range of 20 ksi(138 MPa), the maximum stress would be limited to 34 ksi(235 MPa) with grade C rods''.

Sucker Rod Corrosion

Corrosion significantly affects the fatigue performance of sucker rod steels yet the conditions which can lead to corrosion in operating wells are not fully understood. Because corrosion is frequently observed in casing and tubing strings, the occurrence of corrosion in sucker rod strings is sometimes automatically assumed. These assumptions are often reinforced when water formed scale

---

'' The ultimate tensile stress is assumed to be 105 ksi(724 MPa) in this example.

deposits are mistaken for corrosion products (Couch,1981). But in contrast to casing and tubing strings, in which corrosion can also occur as a result of low pH condensate and sulphate reducing bacteria (NACE,1976), corrosion of sucker rod strings only occurs when specific conditions make the brine corrosive to the rods.

The specific conditions which lead to corrosive brines were in question for many years (Copson,1951), but recent studies (Bonis & Crolet,1983) (Martin,1983) have shown that both low pH due to dissolved CO_2 and high oxidizing potential due to dissolved O_2 are key factors. Previous studies (Shock & Sudbury,1951) (Rogers & Shellshear,1937) demonstrated that a pH of 4.5 was required for corrosion of steel to occur in the presence of CO_2 (Shock) and a less acid pH of 5.4 also resulted in corrosion if traces of H_2S were present (Rogers). These results seemed to rule out pH as a factor in sucker rod corrosion since well-head pH was seldom below 6.4 (Shock). However, Bonis & Crolet (1983) examined pH as a function of CO_2 partial pressure, temperature, and buffer salt concentrations and subsequently determined that downhole pH of the brine could reach 5.0 in some specific instances.

Martin (1983) studied the role of dissolved O_2 in downhole corrosion. Though untouched reservoirs were known to be free of dissolved O_2, Martin suggested that contamination of producing reservoirs with air was more common than previously thought. In support of his

hypothesis, Martin observed that oxygen could be partially reacted by naturally occurring reducing agents in the oil well fluids. In this intermediate state, the oxygen could not be detected by conventional methods nor could it be removed by oxygen scavengers yet it retained much of its oxidizing potential.

In conclusion, both low pH brines and oxidizing brines probably play a role in sucker rod corrosion though research is required to determine the prevalence of these factors in operating wells.

Effects of Damaging Environments

Introduction

The importance of crack initiation in the sucker rod failure process was outlined in the first part of this appendix. Crack initiation can occur by regular fatigue mechanisms, by mechanical damage, by existing manufacturing flaws or by the simultaneous action of stress in a damaging environment. This section will examine this last mechanism of crack initiation from the perspective of corrosion fatigue, pitting attack and sulphide stress cracking (SSC).

Corrosion Fatigue

Corrosion fatigue is a general process that occurs when metal is exposed simultaneously to corrosion and cyclic stresses. In high cycle fatigue, the main result is an acceleration of crack initiation (Duquette & Laird,1972) with a resultant reduction in the fatigue life. The combined

effects of corrosion and fatigue are much greater than the separate sum of their effects (Wescott,1948).

Though S-N charts are used to describe fatigue life in corrosive environments, the results must be carefully interpreted. Crack initiation in damaging environments is not only a function of stress fluctuations, but is also a function of the exposure time and the exact environmental conditions. Therefore each S-N chart will be specific for the cycling frequency and the conditions under which the tests were conducted. This is an important consideration if the results of short-term high-frequency tests are extrapolated to long-term low-frequency applications. Not only will the cycles to failure be reduced, but the mechanism of crack initiation may be completely different. One generalized finding of S-N charts dealing with corrosive environments is the absence of an endurance limit; failure will eventually occur at any stress amplitude. Arbitrarily, the stress amplitude causing a 50% chance of failure at ten million cycles is sometimes taken as the corrosion fatigue limit (Zaba,1962).

Wescott (1938) was the first to examine the possibility of corrosion fatigue within oil well environments. Wescott and subsequent researchers (Jaske & others,1981) studying corrosion fatigue in aerated salt water, found that alloy content, heat treatments, and the ultimate tensile strength had little influence on the corrosion fatigue limit of carbon and medium alloy steels. In severe corrosion under a

fully reversed bending load, the corrosion fatigue limit (ten million cycles) of steels was consistently around 10 ksi(69 MPa).

Wescott (1949) also observed evidence of corrosion fatigue in neutral unaerated oil well waters but the findings were contradicted by later researchers who found no evidence of corrosion fatigue unless medium strength acids or oxygen were present (Mehdizadeh,1974,Duquette & Ulhig,1968). It is possible that Wescott was not as successful in eliminating air from the test environments.

The work of Ulhig & others (1968,1969,1972) was key in establishing the relationship between corrosion and high cycle corrosion fatigue. The findings showed the existence of a critical general corrosion rate below which corrosion had no effect on the fatigue life. Corrosion rates above the critical rate showed progressively greater effects in reducing the fatigue life until a limiting effect was reached at ten to twenty times the critical rate. Beyond this point further increases in the corrosion rate did not result in further reductions of the fatigue performance.

At 1800 cpm(30 hz) (Ulhig), the critical corrosion rate in steel corresponded to the removal of one layer of atoms every five minutes. The researchers proposed that the corrosion process unlocks surface dislocations by preferentially dissolving the newly exposed atoms at these points. The net result is a surface softening allowing an acceleration of the normal fatigue process of crack

initiation and a disappearance of the endurance limit.

The experimental studies of Ulhig discounted both pitting attack and hydrogen attack as factors in high cycle corrosion fatigue. The presence or absence of pitting had no influence on the observed fatigue life in corrosion fatigue. When pitting did occur at a crack it was found to be the result of crevice corrosion occuring after the crack had been initiated. If atomic hydrogen played a role in high cycle corrosion fatigue, cathodic protection which results in the generation of hydrogen should not have been of benefit. In contrast, cathodic protection resulted in a full restoration of the non-corrosive fatigue life and endurance limit.

The work by Ulhig & others did not examine the effects of cyclic frequency on corrosion fatigue. Since sucker rods operate at much lower frequencies, the possibility of other types of environmental damage cannot be ruled out.

In summary, general corrosion can result in a major reduction in the fatigue life along with a removal of the endurance limit. When corrosion fatigue is present, reductions in both the mean stress and the stress range will always result in an increased fatigue life no matter how small the original stresses are. Though pitting and hydrogen attack are not the causes of corrosion fatigue, these processes could be alternative forms of environmental attack in low-frequency fatigue situations.

Stress Raisers from Pitting

Pitting corrosion is a localized form of attack in which high corrosion rates in small areas lead to the formation of hemispherical pits. The rest of the surface usually shows no evidence of corrosion.

The extent of pitting can vary widely and depends strongly on the type of steels used and the type of environment to which the steel is exposed. Localized areas of high stress are thought to be more susceptible to pitting attack and also to have an influence on pit geometry. Steels exposed to sour environments are also considered to be more susceptible to pitting (Zaba,1962) (Gupta,1981).

At one time, pitting attack was thought to be a mechanism of crack initiation in corrosion fatigue (Wescott,1948) but pitting is now recognized to be a separate form of environmental damage. A good example of a sucker rod steel that demonstrated good corrosion fatigue performance but poor pitting resistance was the 4140 steel introduced in the 1940's (Bucaram & others,1973). During high-frequency corrosion fatigue tests, the new alloy gave a much superior fatigue life compared to the regular carbon steels. Subsequent use in the field resulted in a shorter fatigue life due to pitting damage which only became apparent during the low-frequency cycling.

Crack initiation from pitting occurs in two basic stages. The first stage is a chemical attack in which pits functioning as stress raisers are formed. Stress plays only

a minor role in this step by somewhat accelerating the process and by influencing pit geometry. In the second stage, a crack is initiated at the base of the stress raiser by regular fatigue processes. The duration of crack initiation will depend both on the geometry and the size of the pit as well as on the cyclic stresses being imposed.

To summarize, pitting attack is a long term process in which pits are formed by local corrosive attack. These pits then act as stress raisers where crack initiation can occur by regular fatigue processes. Crevice corrosion of existing cracks is often mistaken for pitting attack, and ,therefore, the role of pitting in sucker rod failures is not fully known.

Sulphide Stress Cracking

Sulphide stress cracking (SSC) is a failure mechanism in which a steel suddenly fails by brittle fracture after a period of exposure to a static stress in an H_2S environment. The H_2S initiates hydrogen attack on the steel though the exact mechanisms of SSC are unknown (Martin,1974). Though the pH of the H_2S solutions has an influence, SSC can occur at neutral pH conditions (Hudgins & others,1966).

SSC is usually associated with steels having a Rockwell hardness above H_RC 22 (NACE,1975) and which are exposed to static stresses approaching the yield strength of the steel. However, Swanson (& Tresseder,1967) found that some sucker rod steels of low hardness were very susceptible to SSC at stresses below the yield strength. This susceptibility,

combined with the fact that actual rod stresses may be above the assumed design stresses, suggests that SSC cannot be ruled out as a factor in crack initiation in sour wells. Recent findings (Martin,1983) support the possibility that SSC is a factor in rod string failures. Martin reported that the inhibitors that gave the lowest hydrogen penetration rates were also the most effective in reducing sucker rod failures. The inhibitors studied were all equally effective in reducing the general corrosion rate.

In summary, SSC could be a factor in crack initiation processes. If SSC does occur, the time of exposure and the maximum stress may be more important than the number of cycles or the stress range. Proper material selection and reduction of stress levels below a critical value could be possible means of eliminating SSC crack initiation.

Summary

The crack initiation process is the key step in sucker rod failures and results either from purely mechanical means or from mechanical-environmental interactions. The role played by the oil well environment has yet to be fully understood, but it is possible that more than one type of failure mechanism can occur. Except when cracks are created during manufacture or during mishandling of the rods, stress levels play a central role in crack initiation in both damaging and non-damaging environments.

Appendix 3: Least Squares Analysis

The basic problem is to estimate R and θ at a given cross section using a series of vertical deviation measurements, R_i, at the corresponding rotations, α_i. From Fig. II, one can determine the following relation for R_i,

$$R_i = R\cos(\alpha_i - \theta)$$

which can be rewritten as

$$R_i = R\cos\theta\cos\alpha_i + R\sin\theta\sin\alpha_i.$$

Two new constants, A and B, are defined such that

$$A = R\cos\theta \text{ and } B = R\sin\theta.$$

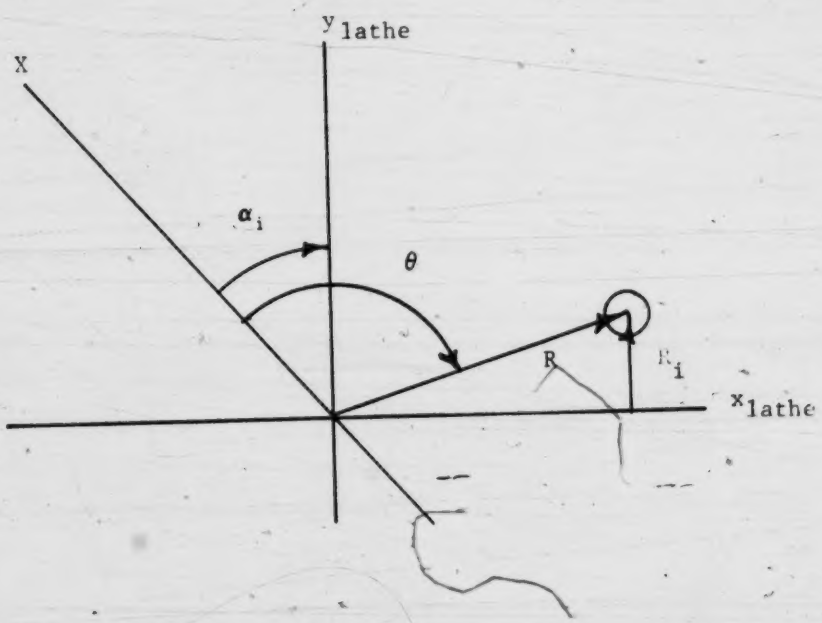

Fig. II. Relationship of α_i and R_i to R and θ

The task of finding R and θ then simplifies to finding the constants A and B such as to minimize the sum of the error squared (least squares fit) in the following equation:

$$R_i = A\cos\alpha_i + B\sin\alpha_i.$$

The solution is obtained by solving the following system of equations (James, 1977) for the coefficients A and B:

$$[F]^T[F]\{c\} = [F]^T\{R_i\}$$

where $\{c\}$ is the coefficient vector, $\{R_i\}$ is the vertical deviation vector and [F] is the following matrix:

$$\begin{bmatrix} \cos\alpha_1 & \sin\alpha_1 \\ \cos\alpha_2 & \sin\alpha_2 \\ \cos\alpha_3 & \sin\alpha_3 \\ \cos\alpha_4 & \sin\alpha_4 \\ \cos\alpha_5 & \sin\alpha_5 \\ \cos\alpha_6 & \sin\alpha_6 \end{bmatrix}.$$

The parameters R and θ can then be found from the following relations:

$$\theta = \text{atan}(B/A) \text{ and } R = B/\sin\theta \text{ or } R = A/\cos\theta.$$

Appendix 4: Difference Equations, Coordinate Transforms, and Program Description

Finite Difference Form of Differential Equation

The finite difference form of the following equation,

1. $$\frac{d^2y}{dz^2} - \frac{P}{EI}\,y = \frac{d^2y_o}{dz^2}.$$

can be derived by integrating the singularity functions (Shigley, 1977) for the rod elements i and i+1 which are adjacent to node i (Fig. III). The singularity function for the moments can be written as

2. $$d^2y/dz^2 = (M/EI_i)\langle z\rangle^0 + \{M/(EI_{i+1}) - M/(EI_i)\}\langle z-h_i\rangle^0.$$

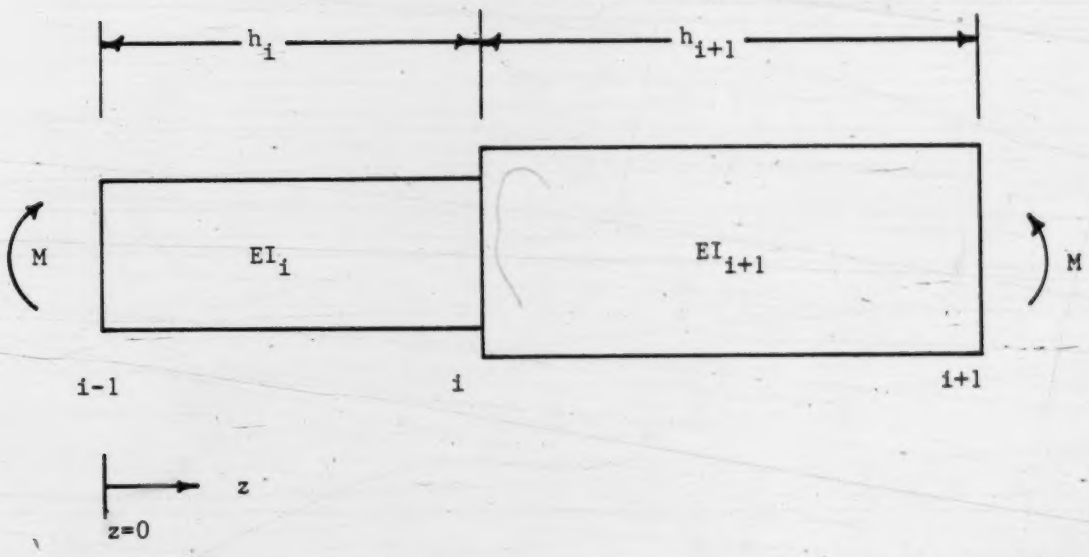

Fig. III. Node i with Adjacent Beam Elements

Integrating twice and solving for the constants gives an expression for $EI\frac{d^2y}{dz^2}$ in terms of the nodal displacements y_{i-1}, y_i, and y_{i+1} as follows:

$$3. \quad EI\frac{d^2y}{dz^2} = \frac{y_{i+1}h_i - (h_i+h_{i+1})y_i + y_{i-1}h_{i+1}}{h_{i+1}h_i(h_iI_{i+1}+h_{i+1}I_i)} 2EI_iI_{i+1}.$$

When I_i equals I_{i+1} and h_i equals h_{i+1}, the finite difference formula reduces to the more familiar central difference equation,

$$4. \quad \frac{d^2y}{dz^2} = \frac{y_{i+1} - 2y_i + y_{i-1}}{h^2}.$$

The last step is to substitute Equation 3. into Equation 1. which, after some rearrangement of terms, results in the final form of the finite difference formulation as follows:

$$\frac{y_{i+1}}{h_{i+1}} + \frac{y_{i-1}}{h_i} - \left[\frac{h_i+h_{i+1}}{h_ih_{i+1}} + \frac{h_iI_{i+1}+h_{i+1}I_i}{2EI_iI_{i+1}}P\right]y_i = \frac{yo_{i+1}}{h_{i+1}} + \frac{yo_{i-1}}{h_i} - \frac{h_i+h_{i+1}}{h_ih_{i+1}}yo_i$$

The finite difference form of the equation for deflections in the x direction is identical to that for the y direction.

The finite difference formulation results in two independent sets of (n-1) simultaneous equations to be solved for y_i and x_i subject to the boundary conditions that both y_i and x_i equal 0 at node 0 and node n. The system of equations is solved by using a Gauss-Seidel iteration method (James, 1977) in which an overrelaxation technique was used to speed convergence. An optimum relaxation parameter of 1.89, determined by trial and error, gave convergence to a

solution within 300 iterations for the 70 element model. The computer subroutine, SOLVE, which is listed at the end of this section, is the actual fortran program used in the solution of the model.

Coordinate Transformations

The first step in transforming the coordinates to a global system is to map the cylindrical coordinates (R, θ, Z) (Fig. 12) of the connected rods to a rectangular coordinate system (Fig. 13) using the following equations for the first rod:

$$x = R_1\cos\theta_1,$$

$$y = R_1\sin\theta_1,$$

$$\text{and } z = -z_1,$$

and the following equations for the second rod:

$$x = R_2\cos(-\theta_2+\text{ANGLE}),$$

$$y = R_2\sin(-\theta_2+\text{ANGLE}),$$

$$\text{and } z = z_2$$

where ANGLE is the rotation angle of the connection between the two rods. The coordinates are then transformed to a global coordinate system, X_G, Y_G, Z_G, (Fig. 13) using a transformation matrix (Paul, 1981) and displacement vector as follows:

$$\begin{bmatrix} n_1 & n_2 & n_3 \\ o_1 & o_2 & o_3 \\ p_1 & p_2 & p_3 \end{bmatrix} \begin{Bmatrix} x-x_o \\ y-y_o \\ z-z_o \end{Bmatrix} = \begin{Bmatrix} x_G \\ y_G \\ z_G \end{Bmatrix}$$

where $\{x_o, y_o, z_o\}$ is the displacement vector to the origin of the global coordinate system and $\{x, y, z\}$ is the coordinate vector being transformed. The component vectors $\{n\}$, $\{o\}$, and $\{p\}$ of the transformation matrix correspond to the respective unit vectors in the X_G, Y_G, and Z_G directions (Paul). A new constant, MAG, representing the magnitude of the vector between the ends of the connected rods along the Z_G axis is defined such that

$$MAG = \{(x_n-x_o)^2 + (y_n-y_o)^2 + (z_n-z_o)^2\}^{1/2}$$

where x_n, y_n, and z_n are the coordinates of the distal end of the connected rod pair. The vector components of $\{p\}$, which lies along the Z_G axis, become

$$p_1 = (x_n-x_o)/MAG,$$
$$p_2 = (y_n-y_o)/MAG, \text{ and}$$
$$p_3 = (z_n-z_o)/MAG.$$

Arbitrarily setting n_2 to be 0 and n_1 to be positive and, furthermore, noting that the vectors are unit vectors and are, also, perpendicular to each other (dot products equal 0) results in the following set of simultaneous equations:

$$n_1p_1 + n_3p_3 = 0,$$
$$n_1o_1 + n_3o_3 = 0,$$
$$o_1p_1 + o_2p_2 + o_3p_3 = 0,$$
$$n_1^2 + n_3^2 = 1, \text{ and}$$

$$o_1^2 + o_2^2 + o_3^2 = 1.$$

Solving the equations gives the remaining components of the transformation matrix as follows:

$$n_3 = -\text{sgn}(p_1)\{1 + (p_3^2/p_1^2)\}^{-1/2},$$

$$n_1 = (1 - n_3^2)^{1/2},$$

$$o_3 = \text{sgn}(\zeta)\{1 + (n_3^2/n_1^2) + \zeta^2\}^{-1/2}$$

where $\zeta = (p_1 n_3 - p_3 n_1)/(p_2 n_1)$,

$$o_1 = -o_3 n_3/n_1, \text{ and}$$

$$o_2 = (1 - o_1^2 - o_3^2)^{1/2}.$$

The transformations are performed by the subroutine TRANCO which is included in the program listings.

Description of Computer Programs

All the programs discussed in this section were compiled with a Fortg compiler on an Amdahl 470V/6 computer using the Michigan Terminal System. The fully documented listings of the programs are included at the end of this appendix.

The numerical model makes use of three major subroutine programs, TRANCO, SUCROD, and SOLVE, which are coordinated by a short controlling program, MAIN. In general, the program MAIN first reads in the rod data and initializes the subroutine parameters. Subsequently, the program calls TRANCO which connects two rods by mapping the coordinates of the bends to a global coordinate system. Next, the subroutine SUCROD is called to derive the physical

characteristics of the rod elements. Finally, the subroutine SOLVE is called to solve the numerical model and output the results.

Dividing the program into independent modules gave a great deal of flexibility in analyzing the rod sample. Major changes in the program action could be easily brought about with relatively minor modifications to MAIN. Each of the program sections is discussed briefly in the following paragraphs. Details of program operations can be found in the documented program listings.

The program MAIN, in addition to calling the subroutines in the proper sequence, must initialize the variables and read in the rod data required in the subroutines. Rod data from the rod sample is read from the permanent files RROD, TROD, and ZROD which contain R, θ, and z, respectively for each point measured on the individual rods. These files are included with the program listings to show the format used. Some of the important parameters initialized by MAIN include the loading vector, P, which contains the list of loads to be solved for along with NUMLD which gives the number of loads; the rod identifiers, IR1 and IR2, which determine which two rods are connected along with ANGLE which gives the rotation angle of connection; and the iteration parameters, NUMITR and RF, which determine the number of iterations along with the relaxation parameter to be used in solving the model.

The subroutine, TRANCO, is the first subroutine called by MAIN. TRANCO constructs the initial displacement vectors in the global coordinate system (Fig. 13) of a connected rod pair, using matrices, R, TH, and ZI which contain the cylindrical coordinates (Fig. 12) of the individual rod deviations. The initial displacements of the rod in the X_G and Y_G directions are output in the vectors X0 and Y0 to the temporary file, -yout. As well, TRANCO outputs the values of z_G for all the nodes to the temporary file, -aout.

After the initial bend of the rod pair is defined by TRANCO, the subroutine SUCROD is called to determine the radius, moment of inertia, and the cross-sectional area for each element in the model. SUCROD uses the nodal z values from the temporary file -aout in determining the characteristics of each element. SUCROD output is diverted to another temporary file, -zout. The number of elements is output first followed by the distance, radius, moment of inertia, and cross-sectional area vectors.

Finally the numerical model constructed by TRANCO and SUCROD is solved by calling the subroutine SOLVE. SOLVE uses the initial deformation data in -yout along with the element characteristics in -zout to solve for the final deflections resulting from the applied loads in the loading vector, P. The resulting stresses and DB are also calculated and output to device 12 (assigned when the program is run to either a file or the terminal). A sample output listing is included with the program listings.

Program Listings

Program MAIN

Subroutine TRANCO

Subroutine SUCROD

Subroutine SOLVE

File RROD

File TROD

File ZROD

Sample Output File

Program MAIN

```
C This is the main routine of the analysis program for
C the measured data.
C
      DIMENSION R(36,12),TH(36,12),ZI(36),IDENT(12),X0(150),
     +Y0(150),Z0(150),P(150)
      CALL FTNCMD('ASSIGN 8=RROD',13)
      CALL FTNCMD('ASSIGN 9=ZROD',13)
      CALL FTNCMD('ASSIGN 10=TROD',14)
      CALL FTNCMD('ASSIGN 12=-OUT',14)
C Initialize arrays of measured values.
      DO 10 I=1,36
      READ (8,15) (R(I,J),J=1,12)
   10 CONTINUE
   15 FORMAT (12F6.1)
      DO 20 I=1,36
      READ (10,15) (TH(I,J),J=1,12)
   20 CONTINUE
      READ (10,25) (IDENT(I),I=1,12)
   25 FORMAT (12A4)
      DO 30 I=1,36
      READ (9,35) ZI(I)
   30 CONTINUE
   35 FORMAT (F5.3)
C Initialize load and solution data
      DATA P/1000.,2000.,3000.,4000.,5000.,
     +6000.,7000.,8000.,9000.,10000.,11000.,
     +12000.,13000.,14000.,15000.,135*0.0/
      NUMITR=300
      RF=1.89
      NLIST=0
      NUMLD=15
      ANGLE=60
      IR1=8
      IR2=7
      FAC1=.001
      FAC2=.001
C
C Main Program section
C
      CALL FTNCMD('$EMPTY -ZOUT',12)
      CALL FTNCMD('$EMPTY -YOUT',12)
      CALL FTNCMD('$EMPTY -AOUT',12)
      WRITE (12,45) IDENT(IR1),IDENT(IR2),ANGLE
      CALL TRANCO(R,TH,ZI,IR1,IR2,ANGLE,FAC1,FAC2,X0,Y0,Z0)
      CALL SUCROD
      CALL SOLVE(NUMITR,RF,NLIST,NUMLD,P)
   45 FORMAT (1X/,' ROD ',A4,' AND ROD ',A4,' AT ',F6.1, -
     +' DEGREES')
      RETURN
      END
```

Subroutine TRANCO

```
      SUBROUTINE TRANCO(R,TH,ZI,IR1,IR2,ANGL1,FAC1,FAC2,X0,Y0,Z0)
C This routine takes the cylindrical coordinates from two
C rods and transforms the coordinates to x,y,z coordinates
C originating at the end of rod 1. The variable angle, contains
C the angle of twist connection between the 2 rods. X0,Y0,
C and Z0 are the output vectors. Output is directed to the
C -zout and -aout arrays.
      DIMENSION R(36,12),TH(36,12),ZI(36),X0(150),Y0(150),Z0(150)
      PI=3.1417532
      ANGLE=ANGL1*PI/180
C Transform cylindrical coordinates to an x,y,z system originating
C at the centre of the two rods.
      DO 10 I=1,36
      R1=R(I,IR1)
      R2=R(I,IR2)
      TH1=TH(I,IR1)
      TH2=TH(I,IR2)
      X0(37-I)=R1*COS(TH1*PI/180)*FAC1
      Y0(37-I)=R1*SIN(TH1*PI/180)*FAC1
      Z0(37-I)=-ZI(I)
      X0(35+I)=R2*COS(-TH2*PI/180+ANGLE)*FAC2
      Y0(35+I)=R2*SIN(-TH2*PI/180+ANGLE)*FAC2
      Z0(35+I)=ZI(I)
   10 CONTINUE
C Determine the transformed coordinates
      AMAG=SQRT((X0(71)-X0(1))**2+(Y0(71)-Y0(1))**2+(Z0(71)-Z0(1))
     +**2)
      Z1=(X0(71)-X0(1))/AMAG
      Z2=(Y0(71)-Y0(1))/AMAG
      Z3=(Z0(71)-Z0(1))/AMAG
      X2=0
      IF (Z1.EQ.0) GOTO 20
      X3=SQRT(1/(Z3*Z3/(Z1*Z1)+1))
      IF (Z1.GT.0) X3=-X3
      GOTO 30
   20 X3=0
   30 X1=SQRT(1-X3*X3)
      IF (Z2*X1.EQ.0) GOTO 40
      ETA=(Z1*X3-Z3*X1)/(Z2*X1)
      Y3=SQRT(1/(ETA*ETA+1+X3*X3/(X1*X1)))
      IF (ETA.LT.0) Y3=-Y3
      GOTO 50
   40 Y3=0
   50 Y1=-X3*Y3/X1
      Y2=SQRT(1-Y1*Y1-Y3*Y3)
C Transform coordinates to initial deformation
C Determine displacement vector
      A1=X0(1)
      A2=Y0(1)
      A3=Z0(1)
C Loop to transform coordinates
      DO 100 I=1,71
      X=X0(I)-A1
```

```
      Y=Y0(I)-A2
      Z=Z0(I)-A3
      X0(I)=X1*X+X2*Y+X3*Z
      Y0(I)=Y1*X+Y2*Y+Y3*Z
      Z0(I)=Z1*X+Z2*Y+Z3*Z
  100 CONTINUE
C Output x0,y0, and z0 arrays
      CALL FTNCMD('ASSIGN 10=-YOUT',15)
      CALL FTNCMD('ASSIGN 11=-AOUT',15)
      NUMEL=70
      NDISP=0
      N=NUMEL+1
      WRITE (11,15) NUMEL
      WRITE (10,15) NDISP
   15 FORMAT (I3)
      DO 110 I=1,N
      WRITE (10,35) X0(I),Y0(I)
      WRITE (11,35) Z0(I)
  110 CONTINUE
   35 FORMAT (2E14.7)
      RETURN
      END
C ***********************************************
```

Subroutine SUCROD

```
      SUBROUTINE SUCROD
C This subroutine uses the z array stored in -Aout
C to create R, XI, and Area arrays which are stored
C interleaved with Z on device 8 which is assigned
C file -Zout.
      DIMENSION Z(150),R(150),AREA(150),XI(150)
C Assign input and output files
      CALL FTNCMD('ASSIGN 9=-Aout',14)
      CALL FTNCMD('ASSIGN 8=-Zout',14)
C Input parameters
      READ (9,5) NUMEL
    5 FORMAT (I3)
      N=NUMEL+1
      DO 10 I=1,N
      READ (9,15) Z(I)
   10 CONTINUE
   15 FORMAT (E14.7)
C Initialize parameters
      PI=3.141592
      DIA=.75
      COUDIA=1.625
      WRSQR=1.0
      ZCEN=Z((NUMEL/2)+1)
      Z1=2.0
      Z2=2.375
      Z3=4.1875
      Z4=5.625
C Loop to calculate R,XI, and Area arrays
      DO 20 I=2,N
      ZZ=ABS((Z(I)+Z(I-1))/2-ZCEN)
      IF (ZZ.LT.Z1) GOTO 100
      IF (ZZ.LT.Z2) GOTO 200
      IF (ZZ.LT.Z3) GOTO 300
      IF (ZZ.LT.Z4) GOTO 400
      R(I)=DIA/2.0
      XI(I)=R(I)**4*PI/4
      AREA(I)=R(I)*R(I)*PI
      GOTO 20
  100 R(I)=COUDIA/2.0
      XI(I)=R(I)**4*PI/4
      AREA(I)=R(I)*R(I)*PI
      GOTO 20
  200 R(I)=(COUDIA-.125)/2
      XI(I)=R(I)**4*PI/4
      AREA(I)=R(I)*R(I)*PI
      GOTO 20
  300 R(I)=WRSQR/2
      XI(I)=WRSQR**4/12
      AREA(I)=WRSQR*WRSQR
      GOTO 20
  400 DIS=ZZ-Z3
      R(I)=SHAPE(DIS,DIA)
      XI(I)=R(I)**4*PI/4
```

```
      AREA(I)=R(I)*R(I)*PI
   20 CONTINUE
C Initialize first element of arrays
      R(1)=0
      XI(1)=0
      AREA(1)=0
C Output number of elements
      WRITE (8,25) NUMEL
   25 FORMAT (I3)
C Output arrays
      DO 30 I=1,N
      WRITE (8,35) Z(I),R(I),XI(I),AREA(I)
   30 CONTINUE
   35 FORMAT (4E14.7)
      RETURN
      END
C ************************************************
      FUNCTION SHAPE(X,DIA)
C X IS THE DISTANCE FROM
C THE TOP OF THE CURVE
C DIA IS THE ROD DIAMETET
C IN INCHES.
C ***************
C THIS FUNCTION CALCULATES
C THE DIAMETER OF THE
C ROD AT ANY POINT
C ALONG THE CURVED
C SECTION.
      X1=X
      X2=X*X1
      X3=X*X2
      X4=X*X3
      X5=X*X4
      X6=X*X5
      X7=X*X6
      X8=X*X7
      X9=X*X8
      X10=X*X9
      X11=X*X10
      Y=34.5354+36.61*X1-232.1043*X2+322.286*X3-125.317*X4
      Y=Y-46.3129*X5+48.9632*X6-36.4274*X7+3.5325*X8
      Y=Y+25.3138*X9-9.57848*X10-1.19452*X11
      SHAPE=Y/25.4*DIA/.75/2
      RETURN
      END
```

Subroutine SOLVE

```
      SUBROUTINE SOLVE(NUMITR,RF,NLIST,NUMLD,P)
C This subroutine solves by weighted iteration,
C the problem of a bent rod under tension. Data
C about the rod characteristics are put in numel and
C arrays z, r, xi, and area from the file -zout.
C Data about the geometry of the bend is input
C into ndisp,x0, y0, ydisp, xdisp from the file -yout.
C Data about the loads to be tested
C are input into numld and array p from file load.
C   * output *
C Data is output into arrays smax and stheta, and
C also into sf, sa, st, z(m), p(j). These arrays
C are written to device 12.
      DIMENSION X0(150),Y0(150),XDISP(150),YDISP(150)
      DIMENSION Z(150),R(150),XI(150),AREA(150)
      DIMENSION P(150),H(150),X(150),Y(150),D2X0(150),D2Y0(150)
      DIMENSION A1(150),SBEND(150),SAXIAL(150),STHETA(150)
C Set input files to device numbers
      CALL FTNCMD('ASSIGN 8=-ZOUT',14)
      CALL FTNCMD('ASSIGN 9=-YOUT',14)
C Read solution parameters
      READ (8,15) NUMEL
      READ (9,15) NDISP
   15 FORMAT (I3)
      N=NUMEL+1
C Read the rod deformations
      DO 10 I=1,N
      READ (9,35) X0(I),Y0(I)
   10 CONTINUE
      IF (NDISP.EQ.0) GOTO 12
      DO 11 I=1,N
      READ (9,35) XDISP(I),YDISP(I)
   11 CONTINUE
   12 CONTINUE
   35 FORMAT (4E14.7)
C Read the rod characteristics
      DO 20 I=1,N
      READ (8,35) Z(I),R(I),XI(I),AREA(I)
   20 CONTINUE
C Initialize x and y vectors
      IF (NUMLD.EQ.1) GOTO 38
      DO 40 I=1,N
      X(I)=X0(I)
      Y(I)=Y0(I)
   40 CONTINUE
      GOTO 41
   38 CONTINUE
      DO 39 I=1,N
      X(I)=0
      Y(I)=0
   39 CONTINUE
   41 CONTINUE
C Intialize h vector
```

```
      DO 50 I=2,N
      H(I)=Z(I)-Z(I-1)
   50 CONTINUE
C Initialize initial curvature vectors
      DO 60 I=2,NUMEL
      D2Y0(I)=Y0(I+1)*H(I)-(H(I)+H(I+1))*Y0(I)+Y0(I-1)*H(I+1)
      D2X0(I)=X0(I+1)*H(I)-(H(I)+H(I+1))*X0(I)+X0(I-1)*H(I+1)
   60 CONTINUE
C Intialize variable E
      E=30000000.0
C
C Main Program Solving
C
C Loop for each solution for each load
      WRITE (12,57)
      WRITE (12,58)
      DO 100 J=1,NUMLD
C Initialize A1 constant vector
      DO 110 I=2,NUMEL
      A1(I)=H(I)+H(I+1)+P(J)*H(I)*H(I+1)*(H(I)*XI(I+1)+H(I+1)*XI(I))
     +/(2.0*E*XI(I+1)*XI(I))
  110 CONTINUE
C Iterate for solution given a particular load
      DO 120 K=1,NUMITR
C Calculate at each node
      IF (NDISP.EQ.0) GOTO 128
      DO 130 I=2,NUMEL
      X(I-1)=X(I-1)+XDISP(I-1)
      Y(I-1)=Y(I-1)+YDISP(I-1)
      X(I+1)=X(I+1)-XDISP(I+1)
      Y(I+1)=Y(I+1)-YDISP(I+1)
      Y(I)=RF*(Y(I+1)*H(I)+Y(I-1)*H(I+1)-D2Y0(I))/A1(I)-(RF-1)
     +*Y(I)
      X(I)=RF*(X(I+1)*H(I)+X(I-1)*H(I+1)-D2X0(I))/A1(I)-(RF-1)
     +*X(I)
      X(I-1)=X(I-1)-XDISP(I-1)
      Y(I-1)=Y(I-1)-YDISP(I-1)
      X(I+1)=X(I+1)+XDISP(I+1)
      Y(I+1)=Y(I+1)+YDISP(I+1)
  130 CONTINUE
      GOTO 120
  128 CONTINUE
      DO 129 I=2,NUMEL
      Y(I)=RF*(Y(I+1)*H(I)+Y(I-1)*H(I+1)-D2Y0(I))/A1(I)-(RF-1)
     +*Y(I)
      X(I)=RF*(X(I+1)*H(I)+X(I-1)*H(I+1)-D2X0(I))/A1(I)-(RF-1)
     +*X(I)
  129 CONTINUE
  120 CONTINUE
C Section to compute stresses
      DO 140 I=2,N
      SX=P(J)*(X(I)+X(I-1))*R(I)/(2*XI(I))
      SY=P(J)*(Y(I)+Y(I-1))*R(I)/(2*XI(I))
      SBEND(I)=SQRT(SY*SY+SX*SX)
```

```
      SAXIAL(I)=P(J)/AREA(I)
      STHETA(I)=ATAN2(SY,SX)*180/3.141592+180
      IF (STHETA(I).LT.0.0) STHETA(I)=360+STHETA(I)
  140 CONTINUE
      M=MXSUB(SBEND,SAXIAL,N/2,2)
      SFAC=SBEND(M)/SAXIAL(M)
      STRESS=SAXIAL(M)+SBEND(M)
      DIS=30-(Z(M)+Z(M-1))/2
      M1=MXSUB(SBEND,SAXIAL,N,N/2)
      SFAC1=SBEND(M1)/SAXIAL(M1)
      STRES1=SAXIAL(M1)+SBEND(M1)
      DIS1=(Z(M1)+Z(M1-1))/2-34
C Section to output stresses.
   57 FORMAT (' LOAD DISTANCE ANGLE NODE STRESS',
     +' STRESS STRESS STRESS')
   58 FORMAT (' (LB) (INCHES) (DEG) (PSI) ',
     +' (AXIAL) (BEND) FACTOR')
      WRITE (12,55) P(J),DIS,STHETA(M),M,STRESS,SAXIAL(M),SBEN
     +D(M),SFAC
      WRITE (12,55) P(J),DIS1,STHETA(M1),M1,STRES1,SAXIAL(M1),
     +SBEND(M1),SFAC1
   55 FORMAT (F8.0,F8.2,F8.1,I8,F8.0,F8.0,F8.0,F8.3)
      IF (NLIST.NE.1) GOTO 100
      WRITE (12,61)
      DO 150 I=2,N
      ZDIS=(Z(I)+Z(I-1))/2.0
      SFAC=SBEND(I)/SAXIAL(I)
      WRITE (12,59) ZDIS,STHETA(I),SAXIAL(I),SBEND(I),
     +SFAC
   59 FORMAT (F10.2,F10.1,F10.0,F10.0,F10.3)
   61 FORMAT (1X/,' DISTANCE',' ANGLE ','AXIAL STR ',
     +' BEND STR ','STRESS FAC')
  150 CONTINUE
  100 CONTINUE
      RETURN
      END
C
C Function programs
C
C Function to return subscript of maximum stress
      FUNCTION MXSUB(S,A,N,NSTART)
      DIMENSION S(150),A(150)
      AMX=0
      DO 10 I=NSTART,N
      IF (S(I)+A(I).LE.AMX) GOTO 10
      AMX=S(I)+A(I)
      M=I
   10 CONTINUE
      MXSUB=M
      RETURN
      END
```

File RROD

0.0	0.0	0.0	0.0	0.0	0.0	0.0	0.0	0.0	0.0	0.0	0.0
0.0	0.0	0.0	0.0	0.0	0.0	0.0	0.0	0.0	0.0	0.5	0.0
0.0	0.0	0.0	0.0	0.0	0.0	0.0	0.0	0.0	0.0	1.0	0.0
0.0	0.0	0.0	0.0	0.0	0.0	0.0	0.0	0.0	0.0	1.5	0.0
3.6	2.1	1.5	0.8	2.5	2.0	2.2	4.5	3.8	4.7	2.1	0.0
2.6	10.7	18.5	14.4	14.0	14.6	9.1	18.0	13.5	20.4	2.7	0.0
3.9	9.8	15.4	13.7	12.9	13.8	11.0	20.4	11.8	18.7	3.0	0.0
5.0	8.9	13.5	13.4	11.7	12.8	11.1	19.3	10.8	18.1	3.3	0.0
6.1	8.1	11.6	13.2	10.6	11.9	11.2	18.2	9.9	17.6	3.5	0.0
7.1	5.9	10.1	12.3	10.9	10.8	11.2	16.3	8.2	17.1	3.8	0.0
11.2	6.3	9.7	13.8	8.5	7.9	11.5	14.9	9.9	16.6	4.1	0.0
9.9	8.2	8.9	11.1	15.3	7.7	7.4	22.0	5.5	16.1	4.5	0.0
11.9	6.5	2.2	16.9	2.0	5.2	10.8	13.3	8.2	13.2	5.0	0.0
13.1	3.1	8.2	19.6	2.2	6.2	15.0	12.0	9.7	11.6	5.5	0.0
13.4	6.1	14.5	22.4	0.7	9.1	18.7	12.2	12.2	12.4	6.0	0.0
15.5	7.3	21.9	24.8	3.0	11.5	17.9	12.0	15.5	15.6	6.5	0.0
18.3	9.4	31.4	28.3	5.1	15.1	20.0	10.9	18.1	18.9	7.0	0.0
24.4	11.9	48.7	35.7	9.5	23.6	25.4	10.7	25.7	25.0	8.0	0.0
31.8	15.0	67.3	44.2	15.5	32.3	35.7	10.3	32.0	30.5	9.0	0.0
38.8	18.9	83.6	54.1	20.7	41.0	46.3	10.2	42.5	37.0	10.0	0.0
45.8	23.4	97.4	62.9	26.4	50.1	55.2	11.0	48.8	42.9	11.0	0.0
52.8	28.3	111.4	72.3	33.2	59.3	64.9	11.0	59.2	48.8	12.0	0.0
61.0	34.0	125.1	79.9	42.4	68.8	74.6	12.3	68.0	54.3	13.0	0.0
67.9	38.8	139.5	89.9	51.9	78.7	83.8	13.2	77.7	60.3	14.0	0.0
75.4	45.0	154.8	98.8	62.2	89.1	92.9	14.0	87.2	65.2	15.0	0.0
82.5	50.9	169.4	107.6	72.3	99.2	101.2	15.8	96.9	70.6	16.0	0.0
89.2	58.0	184.1	118.1	81.4	109.7	110.1	16.3	106.3	76.9	17.0	0.0
95.8	64.0	198.6	128.0	90.4	120.6	118.2	18.0	114.9	82.4	18.0	0.0
102.5	70.8	213.2	139.0	98.2	130.8	127.5	19.9	125.7	88.6	19.0	0.0
108.6	77.3	229.3	147.3	104.9	140.0	134.7	21.7	135.6	94.4	20.0	0.0
121.4	90.7	261.0	168.4	119.2	159.8	151.5	24.8	155.6	104.8	22.0	0.0
134.5	104.0	291.8	187.1	131.5	178.9	168.3	28.3	174.5	111.9	24.0	0.0
147.9	116.9	322.0	209.0	142.4	198.0	185.6	31.7	195.0	118.3	26.0	0.0
160.5	129.7	352.9	227.5	155.0	218.0	202.5	35.0	212.6	125.2	28.0	0.0
174.2	141.0	383.8	246.0	165.6	236.0	220.5	41.3	231.0	131.7	30.0	0.0
187.1	151.0	414.8	269.7	176.5	255.6	238.2	47.3	251.3	138.4	32.0	0.0
3b	4b	5a	1b	1a	5b	3a	4a	2a	2b		

This file contains the maximum radius of bend at each z location measured. The units are thousandths of an inch.

File TROD

0.0	0.0	0.0	0.0	0.0	0.0	0.0	0.0	0.0	0.0	0.0	0.0
0.0	0.0	0.0	0.0	0.0	0.0	0.0	0.0	0.0	0.0	0.0	0.0
0.0	0.0	0.0	0.0	0.0	0.0	0.0	0.0	0.0	0.0	0.0	0.0
0.0	0.0	0.0	0.0	0.0	0.0	0.0	0.0	0.0	0.0	0.0	0.0
327.0	3.0	27.0	53.0	123.0	48.0	9.0	358.0	153.0	47.0	0.0	0.0
1.0	127.5	131.0	301.5	228.5	165.0	68.0	294.0	266.0	28.0	0.0	0.0
1.5	135.5	124.5	309.0	225.0	166.0	76.0	292.0	261.0	27.5	0.0	0.0
356.5	137.5	127.5	314.0	224.5	161.7	78.2	295.2	258.2	29.2	0.0	0.0
349.5	139.5	130.5	319.0	224.0	157.5	80.5	298.5	255.5	31.0	0.0	0.0
0.0	150.0	135.0	321.0	218.0	148.5	87.5	293.5	254.0	34.5	0.0	0.0
33.0	148.0	125.0	329.0	208.0	147.0	93.0	298.0	212.0	33.0	0.0	0.0
20.0	104.0	170.0	328.0	195.0	147.0	112.0	288.0	186.0	46.0	0.0	0.0

```
38.0  125.0 265.0 331.0 217.0 90.0  108.0 325.0 136.0 35.0   0.0   0.0
22.0  190.0 272.0 351.0 204.0 85.0  107.0 334.0 139.0 57.0   0.0   0.0
18.0  230.0 271.0 357.0 113.0 83.0  114.0 329.0 132.0 70.0   0.0   0.0
7.0   233.0 267.0 6.0   58.0  68.0  113.0 324.0 117.0 75.0   0.0   0.0
358.0 230.0 265.0 10.0  55.0  64.0  101.0 319.0 112.0 76.0   0.0   0.0
349.0 224.0 266.0 22.0  43.0  55.0  75.0  314.0 100.0 79.0   0.0   0.0
345.0 214.0 267.0 32.0  37.0  52.0  62.0  302.0 94.0  77.0   0.0   0.0
342.0 206.0 268.0 39.0  33.0  51.0  56.0  297.0 90.0  77.0   0.0   0.0
340.0 201.0 269.0 42.0  31.0  49.0  52.0  291.0 88.0  77.0   0.0   0.0
340.0 199.0 270.0 46.0  29.0  48.0  50.0  284.0 86.0  76.0   0.0   0.0
338.0 199.0 270.0 46.0  28.0  47.0  47.0  281.0 85.0  75.0   0.0   0.0
337.0 198.0 270.0 47.0  27.0  47.0  45.0  279.0 84.0  75.0   0.0   0.0
337.0 199.0 271.0 48.0  26.0  46.0  44.0  272.0 82.0  73.0   0.0   0.0
336.0 200.0 271.0 49.0  25.0  46.0  42.0  270.0 82.0  72.0   0.0   0.0
336.0 202.0 272.0 50.0  24.0  46.0  41.0  268.0 81.0  71.0   0.0   0.0
336.0 203.0 272.0 51.0  23.0  46.0  40.0  261.0 80.0  70.0   0.0   0.0
336.0 204.0 272.0 52.0  23.0  46.0  39.0  259.0 80.0  68.0   0.0   0.0
336.0 205.0 272.0 53.0  23.0  46.0  38.0  257.0 80.0  67.0   0.0   0.0
335.0 207.0 272.0 54.0  20.0  48.0  36.0  252.0 79.0  66.0   0.0   0.0
335.0 208.0 272.0 56.0  18.0  48.0  34.0  245.0 78.0  64.0   0.0   0.0
335.0 209.0 272.0 58.0  16.0  48.0  33.0  239.0 78.0  63.0   0.0   0.0
335.0 209.0 272.0 59.0  13.0  48.0  31.0  233.0 77.0  62.0   0.0   0.0
333.0 210.0 272.0 60.0  10.0  48.0  29.0  227.0 77.0  61.0   0.0   0.0
333.0 210.0 272.0 62.0  8.0   48.0  28.0  221.0 76.0  60.0   0.0   0.0
3b  4b  5a  1b  1a  5b  3a  4a  2a  2b  AN  ST
This file contains the angles of the maximum bend in the
rods as measured from the coupling with the 3 notches on
it (center notch = 0 degrees).  The format is 10F6.1.
```

File ZROD

```
0.0
0.5
1.0
1.5
2.125
2.75
3.0
3.25
3.5
3.75
4.125
4.5
5.0
5.5
6.0
6.5
7.0
8.0
9.0
10.0
11.0
12.0
13.0
14.0
```

15.0
16.0
17.0
18.0
19.0
20.0
22.0
24.0
26.0
28.0
30.0
32.0

This file gives the z coordinate from the chuck on the lathe for the rods that were measured. Coordinates at 0.0, 0.5, 1.0, 1.5, and 3.25 inches have been added for computational purposes. The deformation at these points must be interpolated.

Sample Output File

ROD 4a AND ROD 3a AT 60.0 DEGREES

LOAD (LB)	DISTANCE (INCHES)	ANGLE (DEG)	NODE	STRESS (PSI)	STRESS (AXIAL)	STRESS (BEND)	STRESS FACTOR
1000.	3.75	33.4	23	3129.	2264.	866.	0.382
1000.	4.25	37.5	51	4418.	2264.	2154.	0.952
2000.	3.75	29.4	23	5685.	4527.	1158.	0.256
2000.	4.25	36.4	51	8075.	4527.	3548.	0.784
3000.	3.75	25.6	23	8064.	6791.	1274.	0.188
3000.	4.25	35.6	51	11430.	6791.	4639.	0.683
4000.	3.75	22.0	23	10368.	9054.	1314.	0.145
4000.	4.25	35.1	51	14618.	9054.	5563.	0.614
5000.	3.75	18.3	23	12635.	11318.	1317.	0.116
5000.	4.25	34.6	51	17697.	11318.	6379.	0.564
6000.	3.75	14.7	23	14880.	13581.	1299.	0.096
6000.	4.25	34.3	51	20698.	13581.	7116.	0.524
7000.	3.75	10.9	23	17113.	15845.	1268.	0.080
7000.	4.25	34.0	51	23638.	15845.	7793.	0.492
8000.	3.75	7.0	23	19338.	18108.	1230.	0.068
8000.	4.25	33.9	51	26531.	18108.	8422.	0.465
9000.	3.75	2.9	23	21560.	20372.	1188.	0.058
9000.	4.25	33.7	51	29383.	20372.	9011.	0.442
10000.	3.75	358.5	23	23781.	22635.	1145.	0.051
10000.	4.25	33.6	51	32202.	22635.	9566.	0.423
11000.	21.00	161.5	6	26035.	24899.	1137.	0.046
11000.	4.25	33.5	51	34991.	24899.	10092.	0.405
12000.	21.00	161.6	6	28358.	27162.	1196.	0.044
12000.	4.25	33.4	51	37754.	27162.	10591.	0.390
13000.	21.00	161.6	6	30676.	29426.	1250.	0.042
13000.	4.25	33.4	51	40495.	29426.	11069.	0.376
14000.	21.00	161.5	6	32990.	31690.	1300.	0.041
14000.	4.25	33.4	51	43214.	31690.	11525.	0.364
15000.	21.00	161.4	6	35299.	33953.	1346.	0.040
15000.	4.25	33.4	51	45916.	33953.	11963.	0.352